Core-annular miscible two-fluid flow in a slippery pipe: A stability analysis

Geetanjali Chattopadhyay, Ranganathan Usha, and Kirti Chandra Sahu

Citation: Physics of Fluids **29**, 097106 (2017); doi: 10.1063/1.4989744
View online: http://dx.doi.org/10.1063/1.4989744
View Table of Contents: http://aip.scitation.org/toc/phf/29/9
Published by the American Institute of Physics

Core-annular miscible two-fluid flow in a slippery pipe: A stability analysis

Geetanjali Chattopadhyay,[1,a)] Ranganathan Usha,[1,b)] and Kirti Chandra Sahu[2,c)]
[1]*Department of Mathematics, Indian Institute of Technology Madras, Chennai 600036, Tamilnadu India*
[2]*Department of Chemical Engineering, Indian Institute of Technology Hyderabad, Kandi, Sangareddy 502285 Telangana, India*

(Received 12 June 2017; accepted 29 August 2017; published online 21 September 2017)

This study is motivated by the preliminary direct numerical simulations in double-diffusive (DD) core-annular flows with slip at the wall which displayed elliptical shaped instability patterns as in a rigid pipe case; however, slip at the pipe wall delays the onset of instability for a range of parameters and increases the phase speed. This increased our curiosity to have a thorough understanding of the linear stability characteristics of the miscible DD two-fluid flow in a pipe with slip at the pipe wall. The present study, therefore, addresses the linear stability of viscosity-stratified core-annular Poiseuille flow of miscible fluids with matched density in a slippery pipe in the presence of two scalars diffusing at different rates. The physical mechanisms responsible for the occurrence of instabilities in the DD system are explained through an energy budget analysis. The differences and similarities between core-annular flow in a slippery pipe and in a plane channel with velocity slip at the walls are explored. The stability characteristics are significantly affected by the presence of slip. The diffusivity effect is non-monotonic in a DD system. A striking feature of instability is that only a band of wavenumbers is destabilized in the presence of moderate to large inertial effects. Both the longwave and shortwave are stabilized at small Reynolds numbers. Slip exhibits a dual role of stabilizing or destabilizing the flow. The preliminary direct numerical simulations confirm the predictions of the linear stability analysis. The present study reveals that it may be possible to control the instabilities in core-annular pressure driven pipe flows by imposing a velocity slip at the walls. *Published by AIP Publishing.*
https://doi.org/10.1063/1.4989744

I. INTRODUCTION

The study of instabilities in core-annular immiscible or miscible flow configurations gains its importance due to its relevance in a number of applications and the details of several aspects of the analysis with respect to both axisymmetric and swirling disturbances are summarized in Refs. 1–3 and the references therein.

Motivated by the curiosity to understand the differences and similarities between miscible core-annular flows in a pipe and those in a plane channel, several researchers[4–7] have conducted linear stability analysis in two-fluid channel flows. Selvam *et al.*[8] have examined the linear stability of variable miscible core-annular flow in a pipe. Their study revealed that the flow is stable at any Reynolds number up to a critical value of viscosity ratio and this is in contrast with the immiscible counterpart which is unstable at any viscosity ratio.[3] The stability properties in pipe flows are different from those observed in plane channel flows with finite interface thickness, when the less viscous fluid is adjacent to the wall. While the plane channel flow is stabilized with respect to single fluid flow, the core-annular flow is destabilized beyond the critical value of viscosity ratio and this is also in contrast with the miscible planar channel flows.[5,7,9] For a pipe flow with more viscous core, the axisymmetric mode is more unstable than the swirl mode which is again different from the single fluid pipe flow, in which the swirl mode is the most unstable one.

The studies on the double-diffusive (DD) effects on the stability properties of the miscible plane channel[10] and core-annular flows[11] clearly demonstrate different characteristics displayed by the two geometries. Sahu[11] has shown that a stable flow configuration in the context of single-component (SC) flows become unstable due to the DD phenomenon. An increase in diffusivity ratio of faster to slower-diffusing scalar enhances the instability. The diffusion and the radial location of the mixed layer display non-monotonic effects on the stability characteristics. This is in contrast to that observed in a single-component (SC) flow of miscible fluids examined by Selvam *et al.*[8] The physical mechanism responsible for DD instability in core-annular pipe flows has been examined and explained by Sahu[11] through an energy budget analysis and an inviscid stability analysis. He shows that the rate of transfer of energy from the basic flow to the perturbations (the Reynolds stress term) and the rate of energy associated with the gradient of viscosity perturbations in the radial direction are responsible for the DD instability. The inviscid analysis reveals that the DD flows in a cylindrical pipe are inviscidly stable. Further, the direct numerical simulation (DNS) results are presented on DD effects in the nonlinear regime, and the simulations reveal an

[a)]Also at Department of Mathematics, Indian Institute of Technology Madras.
[b)]Electronic mail: ushar@iitm.ac.in
[c)]ksahu@iith.ac.in

interesting new type of elliptical shaped instability pattern in the work of Sahu.[11]

As a preliminary investigation, we extended the DNS computations of Sahu[11] by incorporating the slip effects appropriately, and the results revealed (Fig. 1) that the slip at the pipe wall delayed the occurrence of instability in a DD core-annular flow configuration for the range of parameters considered and that the instabilities propagated with greater phase speed (c_r) in a slippery pipe [$\beta_s = 0$; $\alpha_c = 2.11$, $\frac{\omega_{r\max}}{\alpha_c} = c_r = 1.2684$; $\beta_s = 0.05$; $\alpha_c = 2.21$, $\frac{\omega_{r\max}}{\alpha_c} = c_r = 1.3379$; where β_s is the slip parameter and $\omega_{r\max}$ is the real part of the perturbation frequency (ω) when the growth rate (ω_i) is maximum and α_c is the critical wavenumber where this maximum value is attained]. The DNS results with slip effects increased our curiosity to understand the slip effects on the linear stability characteristics of core-annular flows of miscible two-fluid flow in a slippery pipe and it is with this as our objective, the present study has been taken up. Such a study would also provide an opportunity to understand the similarities and differences between the present results in a slippery pipe and the results by Ghosh *et al.*[12,13] in a slippery channel. Ghosh *et al.*[12,13] have considered the linear stability analysis of pressure-driven miscible two-fluid three layer channel flows with slip at the walls of the channel. Their results demonstrated that the slip plays a dual role of either stabilizing or destabilizing the flow in a rigid channel and this in turn provides an effective way to control the flow in such a configuration with viscosity stratification. The present study gains its significance in applications where the walls of the pipe are porous, chemically patterned, or molecular rough surfaces, and which can be modeled and represented by appropriate velocity slip at the walls. What does the slip do? The velocity slip at the wall reduces the flow resistance provided by viscous drag and thus enhances significantly the primary flow distribution near the wall; thereby, slip plays a crucial role on instability behavior.

It is important to note that such investigations have been carried out to assess slip effects in different flow configurations. Note that the slip length measures the surface slip and it is the depth beyond the macroscopic solid surface at which the velocity extrapolates to zero. The slip length is equal in magnitude to the slip velocity per unit shear rate of the flow near a boundary surface, and it can be of the order of 10 nm–10 μm.[14–16] In view of the necessity to understand the effects of slip (arising due to wettability, surface chemistry, and surface roughness), there are reports on the plane Poiseuille flow with both symmetric and asymmetric slip conditions at the walls.[17–20] The linear stability analysis by Lauga and Cossu[20] reveals that the presence of slip at the wall increases the critical value of the Reynolds number significantly. An asymmetric slip condition imposed at the walls by Ling *et al.*[21] shows that the slip plays a dual role of stabilizing/destabilizing the flow without slip and it depends on the slip length. The results for a diverging channel flow, with slip at the wall, examined by Sahu *et al.*[22] showed that the wall slip has a destabilizing influence at low Knudsen numbers, *Kn* (ratio of slip-length to half the local width of the channel). They used the Maxwell slip boundary condition[23] to model the velocity slip at the walls. If the slip wall conditions are used, then the Navier-Stokes equations are valid up to $Kn = 0.1$.[24]

The interface dominated flow of two immiscible fluids in a slippery channel analyzed by You and Zheng[25] shows that the stability of viscosity stratified microchannel flow is enhanced by slip. The slip effects have been observed to be strong (relatively weak) at small and large (close to one) viscosity contrasts. The linear stability of pressure-driven miscible two-fluid three-layer channel flows with slip at the walls of the channel examined by Ghosh *et al.*[12,13] reveal that when the

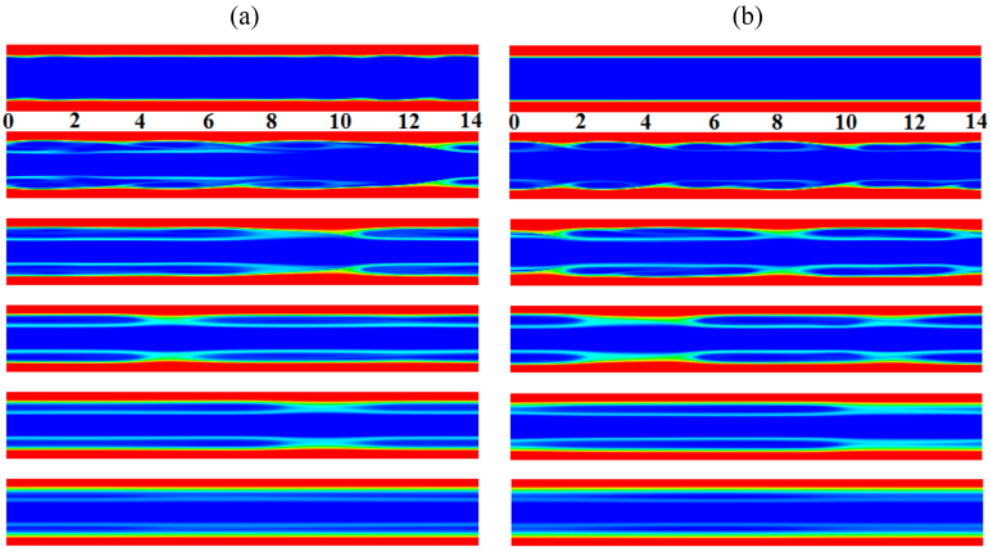

FIG. 1. Evolutions of the slowly diffusing species (s) contour in a DD flow for (a) $\beta_s = 0$ (rigid pipe) and (b) $\beta_s = 0.05$ (slippery pipe) for $\delta = 100$ with other parameters as $Re = 500$, $Sc = 1000$, $q = 0.1$, $R_1 = 0.6$, $R_s = 1$, $R_f = -1.1$. From top to bottom, $t = 100$, 150, 200, 250, 350, and 750. Here, β_s denotes the slip parameter; the other dimensionless parameters are introduced and described in Sec. II. The phase speed = $\frac{\omega_{r\max}}{\alpha_c} = c_r$, where $c_r = 1.2684$ in a rigid pipe and $c_r = 1.3379$ in a slippery pipe. Here $\omega_{r\max}$ denotes the maximum frequency, α_c denotes the critical wavenumber. The results were generated with no slip/slip conditions for the velocity components at the wall of the pipe together with the no-flux conditions for the slowly diffusing (scalar s) and faster diffusing (scalar f) species at the pipe wall and with a periodic boundary condition along the axis of the pipe.

less viscous fluid is adjacent to the slippery walls, the flow is stable for single component (SC) system but is unstable at low Reynolds numbers in the presence of double-diffusive (DD) phenomenon. A new unstable mode (DD mode) distinct from the TS mode arises at Reynolds numbers smaller than the critical Reynolds number for the TS mode, when the mixed layer of the fluids moves towards the slippery walls of the channel. This mode is prominent when the mixed layer overlaps with the critical layer. The velocity slip at the channel wall has a non-monotonic effect on the stability properties of the DD system. The first occurrence of the DD mode is delayed as the slip velocity at the wall increases. In a DD configuration, when the less viscous fluid is placed adjacent to the slippery wall with strong slip effects, the DD system is more stable than the corresponding flow system in a rigid channel. However, for weak slip effects, there exists a region in the α-Re plane, where the DD system in a slippery channel is more unstable than in a rigid channel. There are several investigations on the mechanisms of slip flow past a surface (rough/porous/hydrophobic) in the past decade, which have been reviewed in the studies of Neto *et al.*,[26] Lauga *et al.*,[27] Zhang *et al.*,[28] Rothstein,[29] Kumar *et al.*,[30] Ng *et al.*,[31] and the references therein.

The results of the present study show that slip at the wall of the pipe plays a dual role in the sense that there is either stabilization or destabilization of the flow system with slip as compared to the same configuration without slip. This has relevance in a number of engineering applications where friction reduction of liquid is achieved through effective slip at the wall. In fact, Choi *et al.*[32] have designed the walls of the channel as one with slip and have observed flattening of the velocity profiles within microchannels (nanograted hydrophobic microchannel). They have pointed out that this could be used to reduce the dispersion in microfluidic separation systems. The dual role exhibited by slip is important in scientific and engineering applications as one can design the walls of the pipe either as a hydrophobic/porous or a rough surface with appropriate slip at the wall so as to enhance or inhibit the instability in the considered system (Fig. 2).

The paper is organized as follows: The mathematical formulation and the linear stability analysis are presented in Secs. II and III; the energy budget analysis is presented in Sec. IV; the results for the DD core-annular flow systems in a slippery pipe are discussed in Sec. V; the concluding remarks are given in Sec. VI.

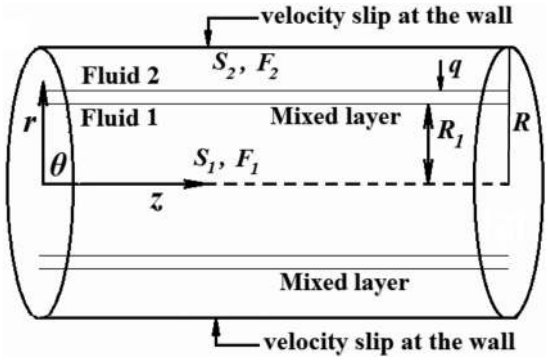

FIG. 2. Schematic diagram of the problem considered. The core ($0 \le r \le R_1$) and the annular ($R_1 + q \le r < R$) regions of the slippery pipe contain fluids "1" and "2," respectively. A mixed layer of thickness q occupies the region $R_1 \le r \le R_1 + q$. There is velocity slip at the walls of the pipe ($r = R$).

II. MATHEMATICAL FORMULATION

We consider the linear stability of pressure-driven core annular, laminar flow of two miscible, incompressible Newtonian fluids of matched densities and different viscosities in a circular tube of radius R, with velocity slip at the walls of the tube. The fluids contain the same solvent but have two species diffusing at different rates; $F(S)$ is the species with high (low) diffusion rate $\mathcal{D}_f$ ($\mathcal{D}_s$). The ratio $\frac{\mathcal{D}_f}{\mathcal{D}_s}$ is denoted by δ ($\delta \ge 1$). The diffusion of the fluids is proportional to the inverse of the Peclet number (Pe), where $Pe = ReSc$. Here Re and Sc are the Reynolds and Schmidt numbers defined in the discussion below. We will also see later that the Peclet number is the ratio of convective to diffusive transport in the species concentration equation. A cylindrical polar coordinate system (r, θ, z), where r, θ, and z denote, respectively, the radial, azimuthal, and axial coordinates, is employed. The concentrations of S and F in fluid 1 of viscosity μ_1 (core fluid; occupying $0 \le r \le R_1$) are S_1 and F_1, respectively. The concentrations of S and F in fluid 2 of viscosity μ_2 (annular fluid; occupying $R_1 + q \le r < R$) are S_2 and F_2, respectively. A mixed layer of uniform thickness q separates the two-fluids and occupies the region $R_1 \le r \le R_1 + q$.[5,8,10–12] The parallel flow approximation (see Appendix C in the work of Sahu[11] for justification) is used in assuming the thickness q to be uniform. As the Reynolds numbers considered in this study are at least of $O(10^2)$, the above assumption is justified unless $Sc \ll 1$. The dynamic viscosity μ of the two fluids is assumed to depend exponentially on the concentration of the solute species,[10]

$$\mu = \mu_1 \exp\left[R_s\left(\frac{S - S_1}{S_2 - S_1}\right) + R_f\left(\frac{F - F_1}{F_2 - F_1}\right)\right], \tag{1}$$

where $R_s = (S_2 - S_1)\frac{\partial(\ln\mu)}{\partial S}$ and $R_f = (F_2 - F_1)\frac{\partial(\ln\mu)}{\partial F}$ are the log-mobility ratios of the slower and faster diffusing scalars S and F, respectively.

The incompressible Navier-Stokes equations along with the convection-diffusion equation for both the scalars are made dimensionless by taking the radius (R) of the pipe as the length scale and $V = \frac{Q}{\pi R^2}$ (Q is the volumetric flow rate) as the velocity scale, ρV^2 and μ_1 as pressure and viscosity scales. The dimensionless governing equations are given by

$$\nabla \cdot \vec{v} = 0, \tag{2}$$

$$\left[\frac{\partial \vec{v}}{\partial t} + \vec{v} \cdot \nabla \vec{v}\right] = -\nabla p + \frac{1}{Re}\nabla \cdot \left[\mu(\nabla \vec{v} + \nabla \vec{v}^T)\right], \tag{3}$$

$$\frac{\partial s}{\partial t} + \vec{v} \cdot \nabla s = \frac{1}{ReSc}\nabla^2 s, \tag{4}$$

$$\frac{\partial f}{\partial t} + \vec{v} \cdot \nabla f = \frac{\delta}{ReSc}\nabla^2 f, \tag{5}$$

where (v_r, v_θ, v_z) denote the dimensionless flow velocity in the r, θ, and z directions, respectively, t is the time, and p denotes the pressure. Here, $Re \equiv \rho VR/\mu_1$, $Sc \equiv \mu_1/\rho\mathcal{D}_s \equiv Pe/Re$ are the Reynolds number and Schmidt numbers, respectively.

The effective Schmidt number of the faster diffusing fluid is Sc/δ.

The dimensionless viscosity is given by

$$\mu = \exp(R_s s + R_f f). \tag{6}$$

When $R_s + R_f > 0\,(<0)$, the flow configuration has more (less) viscous fluid in the annular region than that in the core. $R_s + R_f = 0$ corresponds to a system without viscosity stratification; when either $R_f = 0$ or $R_s = 0$, the configuration corresponds to continuously viscosity stratified single component (SC) system of miscible fluids.

The dimensionless boundary conditions are the Navier slip condition,[33,34] which are given by

$$v_r = 0 \quad \text{on} \quad r = 1, \tag{7}$$

$$v_z = -\beta_s \frac{\partial v_z}{\partial r} \quad \text{on} \quad r = 1, \tag{8}$$

along with the symmetry condition on the center line $r = 0$, given by

$$\frac{\partial v_z}{\partial r} = 0 \quad \text{on} \quad r = 0, \tag{9}$$

where β_s is the dimensionless slip coefficient. In the present study, the focus is on the effects of slip on DD phenomenon related instabilities in core-annular flows that are stable/unstable in a rigid pipe[11] and on the comparison of the present results with miscible double-diffusive flows in a channel with slippery walls.

In the present study, the slip parameter (β_s) values considered are ($0 < \beta_s \leq 0.1$) based on the experimental observations presented in the review by Lauga and Cossu[20] and are the same as those employed in the investigations of a single or immiscible/miscible two-fluid flows in channels with velocity slip at the walls.[12,13,17,20,25,35] The range of β_s used in the computations is realized for a flow in a hydrophobic channel of height ranging from 0.8 μm (40 μm) to 4 μm (200 μm) and corresponds to a slip length of 20 nm (40 nm). It is also worth mentioning here that the experimental measurements of slip lengths corresponding to different solid substrates have been provided by Voronov *et al.*[36] and this is in accordance with the definition of slip proposed by Blake[37] and Vinogradova.[38] In some cases, it is possible that the maximum value of slip length can reach up to 250 μm.

III. LINEAR STABILITY ANALYSIS

The temporal stability of the base flow (see Appendix A) to infinitesimal perturbations is considered in this section. The flow variables are decomposed as a sum of quasi-steady base state and small perturbations as

$$\begin{aligned}(v_r, v_\theta, v_z, p, s, f)(r, \theta, z, t) = {} & (0, 0, U_z(r), P, s_0(r), f_0(r)) \\ & + (i\hat{v}_r, \hat{v}_\theta, \hat{v}_z, \hat{p}, \hat{s}, \hat{f})(r) \\ & \times e^{i(\alpha z + \beta\theta - \omega t)},\end{aligned} \tag{10}$$

where $i = \sqrt{-1}$, α, β are the wavenumbers in the axial and the azimuthal directions, respectively, and $\omega \equiv \alpha c$ is the frequency of the perturbation, c is the complex phase speed ($c = c_r + ic_i$) of the perturbation. Note that αc_i represents the growth of the disturbance amplitude and αc_r gives the phase velocity of the disturbance wave. The flow is linearly unstable if $\omega_i > 0$, stable if $\omega_i < 0$, and neutrally stable if $\omega_i = 0$. The perturbation viscosity is given by $\hat{\mu} = \frac{\partial \mu_0}{\partial s_0}\hat{s} + \frac{\partial \mu_0}{\partial f_0}\hat{f}$. Using the standard procedure,[39] the linearized equations governing the stability problem for the perturbations are obtained [after suppressing the hat (ˆ)] as

$$v_r' + \frac{v_r}{r} + \frac{\beta v_\theta}{r} + \alpha v_z = 0, \tag{11}$$

$$\begin{aligned}-\omega v_r + \alpha v_r U_z = {} & p' - \frac{i}{Re}\left[\mu_0\left\{v_r'' + \frac{v_r'}{r} - \left(\frac{\beta^2+1}{r^2} + \alpha^2\right)\right.\right. \\ & \left.\left. \times v_r - \frac{2\beta}{r^2} v_\theta\right\} + 2\mu_0' v_r' + \alpha U_z' \mu\right],\end{aligned} \tag{12}$$

$$\begin{aligned}-\omega v_\theta + \alpha v_\theta U_z = {} & -\frac{\beta p}{r} - \frac{i\mu_0}{Re}\left\{v_\theta'' + \frac{v_\theta'}{r} - \left(\frac{\beta^2+1}{r^2} + \alpha^2\right)\right. \\ & \left. \times v_\theta - \frac{2\beta}{r^2} v_r\right\} - \frac{i\mu_0'}{Re}\left[v_\theta' - \frac{v_\theta}{r} - \frac{\beta v_r}{r}\right],\end{aligned} \tag{13}$$

$$\begin{aligned}-\omega v_z + U_z' v_r + \alpha U_z v_z = {} & -\alpha p - \frac{i\mu_0}{Re}\left\{v_z'' + \frac{v_z'}{r} - \left(\frac{\beta^2}{r^2} + \alpha^2\right)\right. \\ & \left. \times v_z\right\} - \frac{i\mu_0'}{Re}\left[v_z' - \alpha v_r\right] \\ & - \frac{iU_z'}{Re}\mu' - \frac{i\mu}{Re}\left[U_z'' + \frac{U_z'}{r}\right],\end{aligned} \tag{14}$$

$$-\omega s + s_0' v_r + \alpha U_z s = -\frac{i}{ReSc}\left\{s'' + \frac{s'}{r} - \left(\frac{\beta^2}{r^2} + \alpha^2\right) s\right\}, \tag{15}$$

$$-\omega f + f_0' v_r + \alpha U_z f = -\frac{i\delta}{ReSc}\left\{f'' + \frac{f'}{r} - \left(\frac{\beta^2}{r^2} + \alpha^2\right) f\right\}. \tag{16}$$

In the above equations, a prime denotes differentiation with respect to r. Equations (11)–(16) reduce to the linearized stability equations for the Hagen-Poiseuille flow of a single fluid in a pipe[39] by setting $R_f = R_s = 0$, $\delta = 1$, and $\mu_0 = 1$. The slip boundary condition at the wall of the pipe ($r = 1$) and the symmetry condition at the centerline ($r = 0$) are given by

$$v_r = 0, v_\theta = 0, v_z = -\beta_s \frac{\partial v_z}{\partial r}, s' = 0 \text{ and } f' = 0, \text{ on } r = 1, \tag{17}$$

and

$$\begin{aligned}& v_r = 0, v_\theta = 0, v_z' = 0, p' = 0, s' = 0 \text{ and} \\ & f' = 0 \text{ for } \beta = 0,\end{aligned} \tag{18}$$

$$\begin{aligned}& v_r + v_\theta = 0, 2v_r' + v_\theta' = 0, v_z = 0, p = 0, \\ & s = 0 \text{ and } f = 0 \text{ for } \beta = 1,\end{aligned} \tag{19}$$

$$v_r = 0, v_\theta = 0, v_z = 0, p = 0, s = 0 \text{ and } f = 0 \text{ for } \beta \geq 2. \tag{20}$$

In the absence of slip at the wall, Eqs. (17)–(20) reduce to those of a DD ($R_f + R_s \neq 0$) flow system in a rigid pipe[11] and reduce to those of a SC system when either $R_s = 0$ or $R_f = 0$.

The above system of equations [Eqs. (11)–(16)] and boundary conditions [Eqs. (17)–(20)] constitutes an eigenvalue problem $AX = \omega BX$, and the linear stability characteristics of the flow system are determined by the sign of the eigenvalue, $\omega = \alpha c_i$, which is obtained by solving the dispersion relation

$$F(\alpha, \beta, \omega, Re, Pe, Sc, R_s, R_f, R_1, \delta, \beta_s) = 0. \tag{21}$$

Here $X = (v_r, v_\theta, v_z, p, s, f)$ is the eigenvector and the entries in matrices A and B are presented in Appendix B.

The eigenvalue problem is solved numerically by the public domain software, LAPACK, after discretizing the domain $(0 < r < 1)$ using the Chebyshev spectral collocation method.[40] Large gradients in the mixed layer region are taken care of in the computation by using a sufficiently large number of grid points. This is achieved by using the stretching function[5]

$$r_j = \frac{a}{\sinh(br_0)}\left[\sinh\{(r_c - r_0)b\} + \sinh(br_0)\right], \tag{22}$$

where r_j are the grid point locations, r_c is a Chebyshev collocation point defined by $2r_c = \cos\left\{\left[\frac{\pi(j-1)}{(n-1)}\right] + 1\right\}$, n is the number of collocation points, a is the mid-point of the mixed layer, b is the degree of clustering, and r_0 is given by

$$r_0 = \frac{1}{2b}\ln\left[\frac{1 + (e^b - 1)a}{1 + (e^{-b} - 1)a}\right]. \tag{23}$$

For the range of parameters considered in this study, the computations yielded results that are accurate at least up to five decimal places with $b = 8$.

IV. ENERGY BUDGET ANALYSIS

An energy budget analysis is presented here to facilitate the understanding of the physical mechanism underlying the instabilities that occur due to the DD phenomenon in a slippery pipe. This will help in assessing the role of wall slip on the instabilities that occur in a DD flow in a rigid pipe.[8,11] The derivation is similar to those presented for SC miscible flow systems in a pipe[8] and for a two-dimensional channel[11] and for DD miscible flow systems[12] in a channel. Equations (12)–(14) are, respectively, multiplied by the radial, azimuthal, and axial components of the disturbances in velocity, added, and integrated across the domain $(0 < r < 1)$ to obtain the energy budget equations, given by

$$\dot{\mathcal{E}} = \mathcal{P} - \mathcal{D} + \mathcal{A} + \mathcal{B}_r + \mathcal{B}_z + \mathcal{C}. \tag{24}$$

Here $\dot{\mathcal{E}}$ representing the temporal rate of change of the perturbation kinetic energy is

$$\dot{\mathcal{E}} = \int_0^1 \dot{E} r dr = \omega_i \int_0^1 \left(v_r v_r^* + v_\theta v_\theta^* + v_z v_z^*\right) r dr, \tag{25}$$

and the terms on the right in Eq. (24) are

$$\mathcal{P} = \int_0^1 P_d r dr = \int_0^1 \text{Imag}\left(v_r v_z^*\right) U_z' r dr, \tag{26}$$

the "Reynolds stress" term, which denotes the rate of energy transfer from the base flow to the perturbations, is

$$\begin{aligned}\mathcal{D} = \int_0^1 D r dr = \frac{1}{Re}\int_0^1 \mu_0 \big[& v_r' v_r'^* + v_\theta' v_\theta'^* + v_z' v_z'^* \\ & + \left(\frac{\beta^2}{r^2} + \alpha^2\right)\left(v_r v_r^* + v_\theta v_\theta^* + v_z v_z^*\right) \\ & + \frac{1}{r^2}\left\{v_r v_r^* + v_\theta v_\theta^* + 4\beta\ \text{Real}\left(v_\theta v_r^*\right)\right\}\big] r dr,\end{aligned} \tag{27}$$

which corresponds to the viscous dissipation of energy of the perturbation,

$$\mathcal{A} = \int_0^1 A r dr = \frac{1}{Re}\int_0^1 \frac{\mu_0'}{r}\left(\frac{d}{dr}\left(r v_r v_r^*\right) - v_\theta v_\theta^*\right) r dr, \tag{28}$$

which determines the energy of the perturbations due to mean viscosity gradients,

$$\mathcal{C} = \int_0^1 C r dr = \frac{dP}{dz}\int_0^1 \text{Real}\left(\mu v_z^*\right) r dr, \tag{29}$$

which represents the perturbation energies due to viscosity perturbations and

$$\mathcal{B}_r = \frac{1}{Re}\int_0^1 U_z' \ \text{Real}\left(\mu' z^*\right) r dr, \tag{30}$$

$$\mathcal{B}_z = \frac{1}{Re}\int_0^1 U_z' \ \text{Real}\left(\alpha \mu v_r^*\right) r dr, \tag{31}$$

which are the perturbation energies associated with the gradient of viscosity perturbations in the radial and axial directions, respectively. The new features of the energy equation are the extra terms arising from the interface; it is important to note that these terms in the linearized energy equation incorporate the viscosity stratification effects and slip effects.

V. RESULTS AND DISCUSSION

The effects of velocity slip (β_s) at the pipe wall on the stability characteristics of the flow system in a rigid pipe when the location of the mixed layer (R_1), the ratio of diffusion coefficients of the species (δ), and diffusivity level (Sc) are varied, are examined in this section, for the DD flow configuration. The results are first validated with those obtained by Schmid and Henningson[39] (SH) for Poiseuille flow of a single fluid in a rigid pipe for $Re_{SH} = 2000$. Schmid and Henningson[39] have employed the centerline velocity as a characteristic scale, while the average velocity is used in the present computations. As a result, $Re = 2Re_{SH}$ and $c = 2c_{SH}$. The eigenspectrum is obtained by setting $\delta = 1$ and $R_s = R_f = 0$. The results obtained for different values of axial and azimuthal wavenumbers (α, β) = (1, 0), (0.5, 1), and (0.25, 2) are in good agreement with SH results for the rigid pipe case, namely, the flow is linearly stable at $Re_{SH} = 2000$. Note that SH have reported that the flow is linearly stable for all Reynolds numbers. Further, the growth rates are negative in a slippery pipe ($\beta_s = 0.05, 0.1$) indicating that the flow is also stable for the parameter values mentioned above.

In the case of miscible two-fluid (DD) channel flow with no slip[10]/slip[12] at the walls, the configuration with less viscous fluid near the walls has a stabilizing influence as the base

velocity profile goes away from the inflection profile. This is also true for the SC channel flow systems without or with slip.[5,13] But, the scenario is different in DD rigid pipe flow configurations,[8,11] where the axisymmetric mode and/or swirl mode is/are unstable above a critical viscosity ratio, when the annular fluid is less viscous. It is of interest to see the influence of slip on the instabilities exhibited by the axisymmetric and swirl modes in the DD flow configuration in a rigid pipe. In Sec. V, the results are presented for miscible DD flow in a slippery pipe. Further, the results for both the axisymmetric mode ($\beta = 0$) and the swirl mode ($\beta = 1$) are presented since one of these modes dominates and is more unstable than the higher order modes ($\beta > 1$).

Preliminary results of the DD flow show that it may be possible to either enhance or suppress the growth rates of the axisymmetric modes in the presence of slip (figure not shown); this is true not only when less viscous fluid is in the annular region ($R_f + R_s < 0$) but also when more viscous fluid is in the annular region ($R_f + R_s > 0$). Swirl modes also display similar scenarios in the presence of slip. This motivates us to explore the details of the slip effects in the present study. Further, it is important to understand the physical mechanism that is responsible for different scenarios that are observed in the DD flow system in a slippery pipe, and the explanations are provided through the energy budget analysis (Sec. IV).

A. Influence of location of the mixed layer

The growth rates of the axisymmetric mode ($\beta = 0$) when $Re = 150$ are presented for a flow system with less viscous fluid occupying the annular region ($R_f = -1.1$, $R_s = 1.0$) in Fig. 3(a). The mixed layer is located at $R_1 = 0.75$ and is closer to the pipe wall. The other parameters are fixed as $Sc = 10$, $q = 0.1$, and $\delta = 20$. The DD flow in a rigid pipe ($\beta_s = 0$, solid line) is stable. The presence of slip ($\beta_s = 0.05, 0.07$, and 0.1) destabilizes the flow system for moderate wavenumbers. At this Re(=150), there is a window of unstable wavenumbers, in the presence of slip. The bandwidth of unstable wavenumbers increases with an increase in the slip parameter (β_s).

Why does slip at the wall promote instabilities in the above configuration? Table I presents the details of the energy budget analysis performed for the DD miscible flow system in rigid ($\beta_s = 0$) and slippery ($\beta_s = 0.05, 0.07, 0.1$) pipes for the above flow configuration. The contributions from the different terms in the energy budget analysis as obtained at points A_1, B_1, C_1, and D_1 in Fig. 3(a) are presented. These are the points on the growth rate curves at which the growth rate is

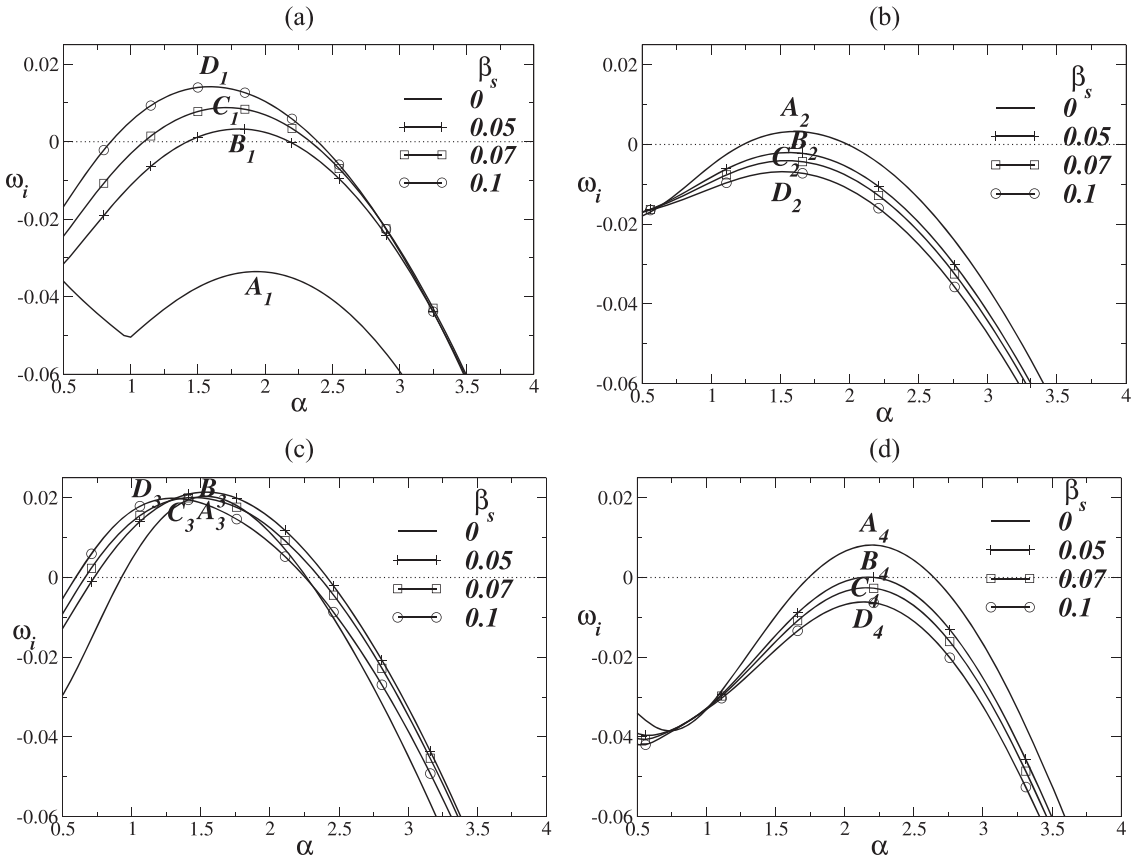

FIG. 3. Growth rates (ω_i) as a function of wavenumber (α) in rigid/slippery pipes with less viscous fluid in the annular region. [(a) and (b)] Axisymmetric mode ($\beta = 0$); [(c) and (d)] swirl mode ($\beta = 1$). In (a) and (c), $R_1 = 0.75$. In (b), $R_1 = 0.425$, and in (d), $R_1 = 0.49$. The other parameters are fixed as $Re = 150$, $\delta = 20$, $Sc = 10$, $R_s = 1$, $R_f = -1.1$, and $q = 0.1$. The solid lines without symbols represent the results in a rigid pipe ($\beta_s = 0$); the solid lines with symbols display the results in a slippery pipe ($\beta_s = 0.05$, $\beta_s = 0.07$, $\beta_s = 0.1$). The SC equivalent flow [$Sc_{eq} = 2Sc/(\delta + 1)$, $R_s = -0.1$, and $R_f = 0$] is stable ($\omega_i < 0$) in this parameter regime. The points A_1, B_1, C_1, and D_1 in (a) correspond to $\alpha = 1.95$, 1.8, 1.7, and 1.6, respectively. The points A_2, B_2, C_2, and D_2 in (b) correspond to $\alpha = 1.61$, 1.56, 1.56, and 1.51, respectively. The points A_3, B_3, C_3, and D_3 in (c) correspond to $\alpha = 1.56$, 1.56, 1.46, and 1.31, respectively. The points A_4, B_4, C_4, and D_4 in (d) correspond to $\alpha = 2.21$, 2.16, 2.16, and 2.16, respectively.

TABLE I. Energy budget for the points A_1, B_1, C_1, and D_1 in Fig. 3(a).

Points	α	ω_i	$\dot{E}$	$\mathcal{P}$	$-\mathcal{D}$	$\mathcal{A}$	$\mathcal{B}_r$	$\mathcal{B}_z$	$\mathcal{C}$
A_1	1.95	−0.033 51	−0.0040	−0.0017	−0.1596	0.0003	0.1671	−0.0058	−0.0043
B_1	1.80	0.003 33	0.0100	−0.0025	−0.1415	0.0003	0.1617	−0.0051	−0.0028
C_1	1.70	0.008 83	0.0124	−0.0034	−0.1351	0.0003	0.1577	−0.0046	−0.0024
D_1	1.60	0.014 21	0.0149	−0.0044	−0.1281	0.0002	0.1532	−0.0040	−0.0020

maximum for that value of β_s. The wavenumber at which it occurs is $\alpha_{A_1} = 1.95$, $\alpha_{B_1} = 1.8$, $\alpha_{C_1} = 1.7$, and $\alpha_{D_1} = 1.6$. The faster diffusing species has a stabilizing role ($R_f = -1.1$); it diffuses faster leaving the slower diffusing species ($R_s = 1$). The net stratification ($R_s + R_f = -0.1$) is negative for the DD flow in a rigid pipe. Note that the positive contribution from $\mathcal{B}_r$ almost balances the contribution from viscous dissipation of energy of perturbation ($\mathcal{D}$) for DD flow in a rigid pipe. The contribution from the rate of energy of the perturbation due to mean viscosity gradients ($\mathcal{A}$), the perturbation energy associated with the viscosity gradient perturbation in the axial direction ($\mathcal{B}_z$), and the perturbation energy that arises due to viscosity perturbation ($\mathcal{C}$) are negligibly small both for DD flow in a rigid pipe and in a slippery pipe. However, the rate of transfer of energy from the basic flow to the perturbations ($\mathcal{P}$, namely, the Reynolds stress) contributes to the temporal rate of change of the perturbation KE which is therefore negative (i.e., $\dot{E}$ is negative) for DD flow in a rigid pipe. As a result, the DD flow in a rigid pipe ($\beta_s = 0$) remains stable for the set of parameters considered [see Fig. 3(a)]. However, in the case of a DD flow in a slippery pipe, the positive contribution from $\mathcal{B}_r$, the rate of perturbation energy associated with the gradient of viscosity perturbation in the radial direction dominates the negative contribution from $\mathcal{D}$ (the rate of viscous dissipation energy of the perturbation) and is thus responsible for the destabilization in this flow system [see Fig. 3(a), $\beta_s = 0.05$, 0.07, 0.1]. It is worth mentioning here that the contribution from $\mathcal{B}_r$ in the energy budget which causes destabilization is due to the nonzero value of $\frac{\partial U_z}{\partial r}$ at the slippery wall. Observe also that an increase in velocity slip corresponds to a decrease in $\mathcal{B}_r$ which results in a reduction in the flow resistance provided by viscous drag. This causes significant enhancement in the primary flow distribution near the wall, and this paves the way for the flow to become unstable in a slippery pipe. In the case of a rigid pipe, $\mathcal{B}_r$ is positive as for a flow configuration in a slippery pipe but is large enough to offer flow resistance arising due to viscous drag, thereby suppresses the base flow distribution near the wall and hence remains stable for the set of parameters considered in this figure. The radial variations of $\dot{E}$, $\mathcal{D}$, P_d, and $\mathcal{B}_r$ are also presented in Figs. 4(a)–4(d), and

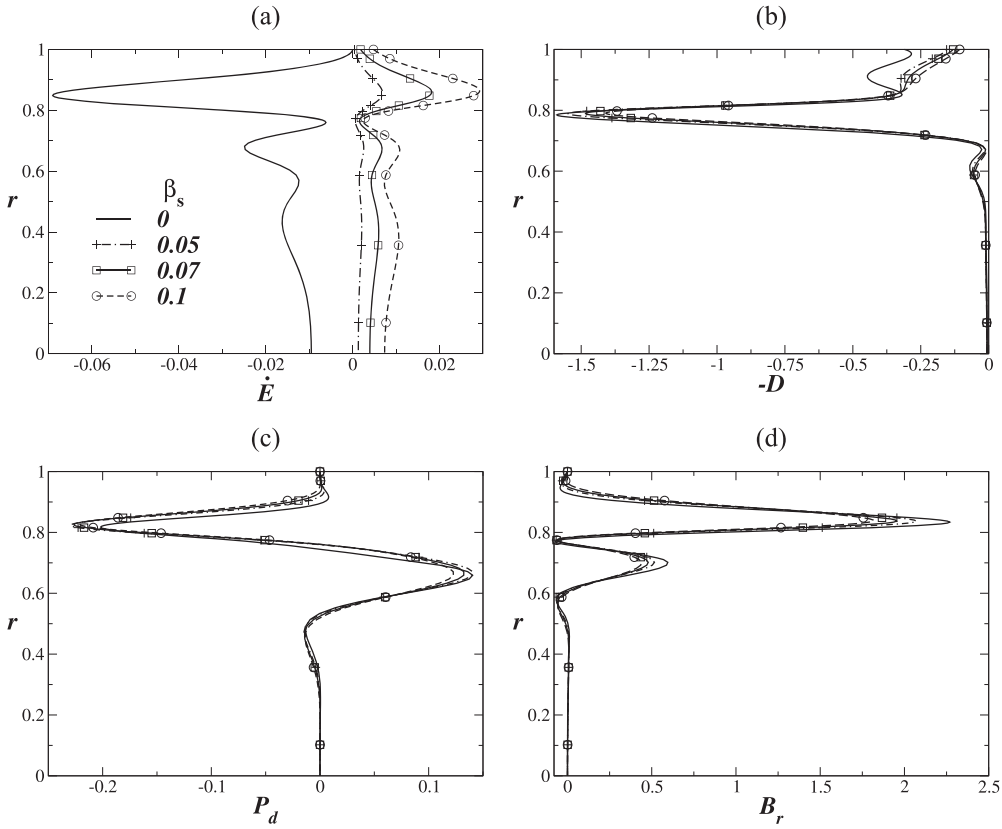

FIG. 4. Radial variations of (a) the rate of change of kinetic energy, $\dot{E}$, (b) the negative of the dissipation rate ($-D$), (c) the production rate, P_d, and (d) B_r of the most dangerous modes at A_1 B_1, C_1, and D_1 in Fig. 3(a) for different values of β_s, respectively. The rest of the parameter values are the same as in Fig. 3(a).

TABLE II. Energy budget for the points A_2, B_2, C_2, and D_2 in Fig. 3(b).

Points	α	ω_i	$\dot{E}$	$\mathcal{P}$	$-\mathcal{D}$	$\mathcal{A}$	$\mathcal{B}_r$	$\mathcal{B}_z$	$\mathcal{C}$
A_2	1.61	0.003 24	0.0005	−0.0020	−0.0739	0.0000	0.0726	−0.0026	0.0063
B_2	1.56	−0.002 03	0.0011	−0.0034	−0.0712	0.0000	0.0718	−0.0026	0.0065
C_2	1.56	−0.004 06	0.0008	−0.0038	−0.0698	0.0000	0.0705	−0.0026	0.0064
D_2	1.51	−0.006 84	0.0003	−0.0042	−0.0661	0.0000	0.0668	−0.0024	0.0062

they clearly show for $\beta_s \neq 0$, the gradient of viscosity perturbations in the radial direction ($\mathcal{B}_r$) gain energy from the mean flow, which results in a destabilization of the flow system in a slippery pipe.

When the location of the interface is moved closer to the centerline [$R_1 = 0.425$; Fig. 3(b)], the slip has a stabilizing effect on the axisymmetric mode. The DD flow in a slippery pipe is more stable than that in a rigid pipe in which the axisymmetric mode exhibits a positive growth rate. Why does slip play a different role in this case? The answer to this is inferred from Table II and Figs. 5(a)–5(d). The rate of viscous dissipation ($\mathcal{D}$) which represents the rate of energy transfer from the perturbation to the mean flow is negative at the mixed layer, near the pipe wall, and also near the centerline [Fig. 5(b)]. The rate of energy transfer from the basic flow to the perturbation $\mathcal{P}$ is negative in the mixed layer [Fig. 5(c)]. However, the rate of energy production associated with the gradient of viscosity perturbation in the radial direction ($\mathcal{B}_r$) is positive [Fig. 5(d), Table II] in the mixed layer and it almost balances the contribution from $\mathcal{D}$. It is seen from Table II that the transfer of energy from base flow to perturbation ($\mathcal{P}$) is negative and it decreases with an increase in β_s. Further, the negative contribution from $\mathcal{B}_z$ is almost the same at all slip parameter values considered. The positive contributions to $\dot{E}$ coming from $\mathcal{C}$ decrease with an increase in β_s. In this case, there is not only positive contribution to the energy budget from the perturbation energies associated with the gradient of viscosity perturbation ($\mathcal{B}_r$) in the radial direction but also from the perturbation energies due to viscosity perturbation ($\mathcal{C}$). This suppresses the basic flow distribution near the wall, and the resistance to flow offered by viscous drag increases, resulting in stabilization of the flow in a slippery pipe. It is again the contribution from $\mathcal{B}_r$. That

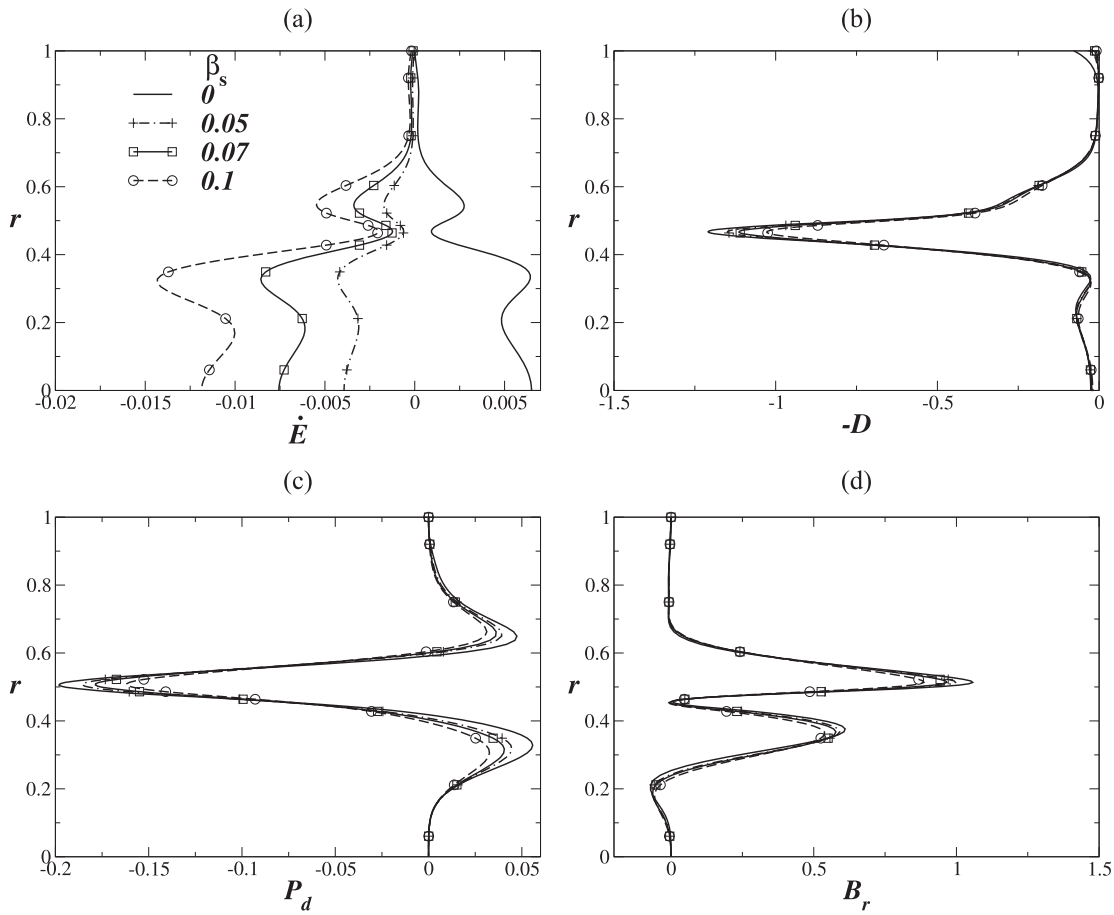

FIG. 5. Radial variations of (a) the rate of change of kinetic energy, $\dot{E}$, (b) the negative of the dissipation rate ($-D$), (c) the production rate, P_d, and (d) B_r of the most dangerous modes at A_2 B_2, C_2, and D_2 in Fig. 3(b) for different values of β_s, respectively. The rest of the parameter values are the same as in Fig. 3(b).

TABLE III. Energy budget for the points A_3, B_3, C_3, and D_3 in Fig. 3(c).

Points	α	ω_i	$\dot{E}$	$\mathcal{P}$	$-\mathcal{D}$	$\mathcal{A}$	$\mathcal{B}_r$	$\mathcal{B}_z$	$\mathcal{C}$
A_3	1.56	0.020 32	0.0068	0.0745	−0.1263	0.0004	0.0529	−0.0012	0.0067
B_3	1.56	0.021 44	0.0098	0.0641	−0.1199	0.0004	0.0585	−0.0010	0.0078
C_3	1.46	0.020 05	0.0094	0.0551	−0.1048	0.0003	0.0516	−0.0007	0.0079
D_3	1.31	0.019 88	0.0093	0.0445	−0.0851	0.0002	0.0421	−0.0003	0.0079

is responsible for stabilization of DD flow in a slippery pipe for the configuration in which the mixed layer is closer to the centerline.

Figure 3(c) shows that the swirl mode ($\beta = 1$) is unstable for the DD configuration with less viscous fluid in the annular region in a rigid pipe. The other parameters are the same as in Fig. 3(a). The growth rates are more for the swirl mode than for the axisymmetric mode in a rigid as well as in a slippery pipe. There is a critical wavenumber α (around $\alpha = 1.4$) below which the DD flow in a slippery pipe has a higher growth rate than that in a rigid pipe. Above this critical α, the growth rates exhibit a non-monotonic trend. The physical mechanism responsible for the scenarios displayed in Fig. 3(c) for the swirl mode can be similarly understood from Table III. The other parameters in Table III are the same as in Table I. Note from Table III that when $R_s = 1$, $R_f = -1.1$, and the mixed layer is nearer the pipe wall, the largest positive contributor to $\dot{E}$ comes from the energy transfer from base flow to perturbations ($\mathcal{P}$). $\mathcal{P}$ decreases with an increase in slip. The total positive contribution ($\mathcal{P} + \mathcal{B}_r$) dominates the rate of dissipation energy of the perturbations, and hence $\mathcal{B}_r$ and $\mathcal{P}$ are responsible for destabilization of DD flow in a rigid as well as in a slippery pipe.

When the mixed layer location is moved closer to the centerline ($R_1 = 0.425$), the swirl mode remains stable in a rigid as well as in a slippery pipe (figure not shown). However, when $R_1 = 0.49$, the scenario is different as seen in Fig. 3(d), namely, the swirl mode for DD flow in a rigid pipe displays a positive growth rate while that in a slippery pipe is stable. In this case ($R_1 = 0.49$), both $\mathcal{P}(>0)$ and $\mathcal{B}_r(>0)$ decrease with an increase in slip for the swirl mode($\beta = 1$) but dominate the viscous dissipation energy of the perturbation, thus resulting in a destabilization of DD flow in a rigid pipe. However, in a slippery pipe, the total contribution from $\mathcal{B}_r + \mathcal{P}$ is insufficient to generate significant base flow distribution near the wall which enhances the resistance to flow by viscous drag, resulting in stabilization of flow in this case. The results in Tables III and IV are also confirmed by the radial variation of $\dot{E}$, $\mathcal{D}$, $\mathcal{B}_r$, and $\mathcal{P}$ but are not shown.

The results show that DD flow in a rigid pipe can be destabilized (stabilized) by wall slip accordingly as the mixed layer is located closer to the wall (nearer the centerline), when the less viscous fluid occupies the annular region, when $Re = 150$.

B. Effects of relative rate of diffusion

It is of interest to know the critical value of Re at which the instability sets in first in the presence of slip and how this critical Reynolds number is affected by changes in the ratio of the diffusion coefficients of the species (δ). With this in view, the neutral stability boundaries in the α-Re plane are presented in Fig. 6(a) for $Sc = 10$, $q = 0.1$, $R_s = 1$, $R_f = -1.1$, $\delta = 20$, and $R_1 = 0.75$. The slip effects are incorporated ($\beta_s = 0$, solid line; $\beta_s = 0.05$, dashed line). The long and short waves are stabilized (axisymmetric mode, $\beta = 0$) for DD flow configurations in a rigid as well as in a slippery pipe, when the less viscous fluid occupies the annular region and the mixed layer is closer to the pipe wall ($R_1 = 0.75$). The unstable region lies inside the enclosed curves. It is clear that finite viscosity contrast and inertial effects are required for the first occurrence of instability in a rigid as well as in a slippery pipe. We observe from Fig. 4 and Table I that at $\delta = 20$, the combined contribution from $\mathcal{B}_r$ and $\mathcal{P}$ is positive and is more than the negative viscous dissipation ($-\mathcal{D}$) in the mixed layer. This enhances the rate of energy transfer from the base flow to the perturbations which is responsible for destabilization of the axisymmetric mode in a DD system. As δ is decreased ($\delta = 10$), the combined positive (figure and table not shown) contribution from $\mathcal{B}_r$, $\mathcal{P}$, and $-\mathcal{D}$ decreases, thereby, increasing the critical Reynolds number of the axisymmetric mode. This effect reveals that an increase in the relative diffusion rate δ enhances instability in a DD system (for rigid as well as slippery pipes). The critical Reynolds number is less for DD flow in a slippery pipe than that in a rigid pipe, indicating the destabilizing role of slip for this set of parameters. In fact, an increase in slip at the wall increases the slope of the base flow profile, thereby suppresses the resistance offered to the flow by viscous forces, resulting in destabilization of the flow system. The bandwidth of unstable wavenumbers is larger for the axisymmetric mode for flow in a slippery pipe as compared to that in a rigid pipe, resulting in a larger unstable region in the α-Re plane.

TABLE IV. Energy budget for the points A_4, B_4, C_4, and D_4 in Fig. 3(d).

Points	α	ω_i	$\dot{E}$	$\mathcal{P}$	$-\mathcal{D}$	$\mathcal{A}$	$\mathcal{B}_r$	$\mathcal{B}_z$	$\mathcal{C}$
A_4	2.21	0.008 095	0.0009	0.0304	−0.0835	0.0002	0.0445	−0.0008	0.0101
B_4	2.16	0.000 069	−0.0003	0.0269	−0.0792	0.0002	0.0424	−0.0006	0.0101
C_4	2.16	−0.002 607	−0.0007	0.0260	−0.0786	0.0002	0.0422	−0.0006	0.0102
D_4	2.16	−0.006 190	−0.0014	0.0247	−0.0778	0.0002	0.0419	−0.0006	0.0102

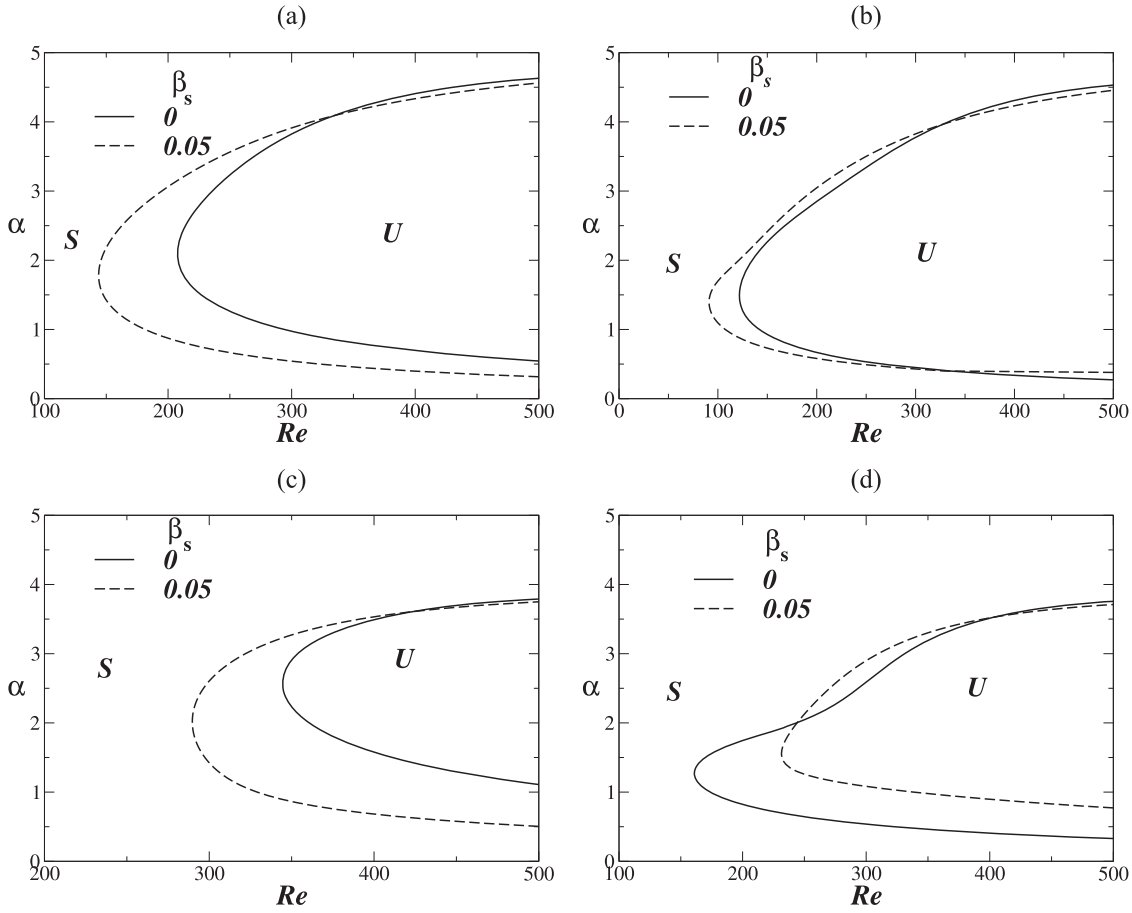

FIG. 6. Effects of slip and the diffusion ratio (δ) on the neutral stability curves in the α-Re plane. The less viscous fluid ($R_s = 1$, $R_f = -1.1$) is nearer to the pipe wall. The mixed layer is located at $R_1 = 0.75$. The other parameters are fixed as $Sc = 10$, $q = 0.1$. [(a) and (c)] Axisymmetric mode ($\beta = 0$); [(b) and (d)] swirl mode ($\beta = 1$) $\delta = 20$ in (a) and (b); $\delta = 10$ in (c) and (d). The solid lines represent the results in a rigid pipe ($\beta_s = 0$); the dashed lines are for flow in a slippery pipe ($\beta_s = 0.05$).

The same scenario is displayed by the swirl mode [$\beta = 1$; Fig. 6(b)]; however, the critical Reynolds number for the swirl mode is lesser than that for the axisymmetric mode; this is so both for the DD flow in a rigid as well as in a slippery pipe. This clearly shows that the swirl mode is more unstable than the axisymmetric mode for the set of parameters considered.

As the diffusivity ratio δ decreases ($\delta = 10$), the axisymmetric mode in the DD flow in a rigid/slippery pipe becomes stable as indicated by the increase in the critical Reynolds number [Fig. 6(c), $(R)_1 = 0.75$]; however, an interesting phenomenon occurs, as seen in Fig. 6(d) for the swirl mode ($\beta = 1$, $\delta = 10$). In this case, the critical Reynolds number in a rigid pipe is smaller than that in a slippery pipe, showing the stabilizing role of slip for the swirl mode. Further, the range of unstable wavenumbers is less for the swirl mode in a slippery pipe.

In what follows, we examine how the location of the mixed layer influences the instability characteristics of the axisymmetric and the swirl modes, in the presence of slip, when the less viscous fluid is nearer to the pipe wall ($R_s = 1$ and $R_f = -1.1$). Figure 7 gives the critical Reynolds number as a function of radial location of the mixed layer (R_1) for different values of δ [$\delta = 10$ in Figs. 7(a) and 7(b); $\delta = 20$ in Figs. 7(c) and 7(d); and $\delta = 100$ in Figs. 7(e) and 7(f)]. The slip effects are incorporated. Figures 7(a), 7(c), and 7(e) present the details for the axisymmetric mode ($\beta = 0$), and Figs. 7(b), 7(d), and 7(f) show the results for the swirl mode ($\beta = 1$). The other parameters are fixed as $Sc = 10$, $q = 0.1$. The critical Reynolds number (Re_{cr}) decreases as the mixed layer is shifted away from the centerline [Figs. 7(a)–7(f)]. Beyond a certain location (say R_{1cr}), which depends on the diffusivity ratio δ, Re_{cr} begins to increase. This demonstrates that the intermediate interface location is the most unstable; the critical Reynolds number is more in a slippery pipe than in a rigid pipe up to R_{1cr} for both the axisymmetric and the swirl modes [Figs. 7(a)–7(f)]. This indicates that when the mixed layer is located nearer to the centerline, the two modes in a slippery pipe are more stable than the corresponding ones in a rigid pipe. Beyond R_{1cr}, the critical Reynolds numbers for the two modes in a rigid pipe are larger than those in a slippery pipe [Figs. 7(a) and 7(c)–7(f)]. Thus, when the mixed layer is located nearer to the pipe wall, slip at the wall tends to destabilize the flow system by advancing the onset of instability. An exception to the above scenario is observed for the swirl mode [Fig. 7(b); $\delta = 10$] when Re_{cr} is more in a slippery pipe than in a rigid pipe for any location of the mixed layer. An increase in the diffusivity ratio results in a decrease in Re_{cr} for both the axisymmetric and the swirl modes, for any location R_1 of the mixed layer which is less than R_{1cr} (that is, when the mixed layer is closer to the

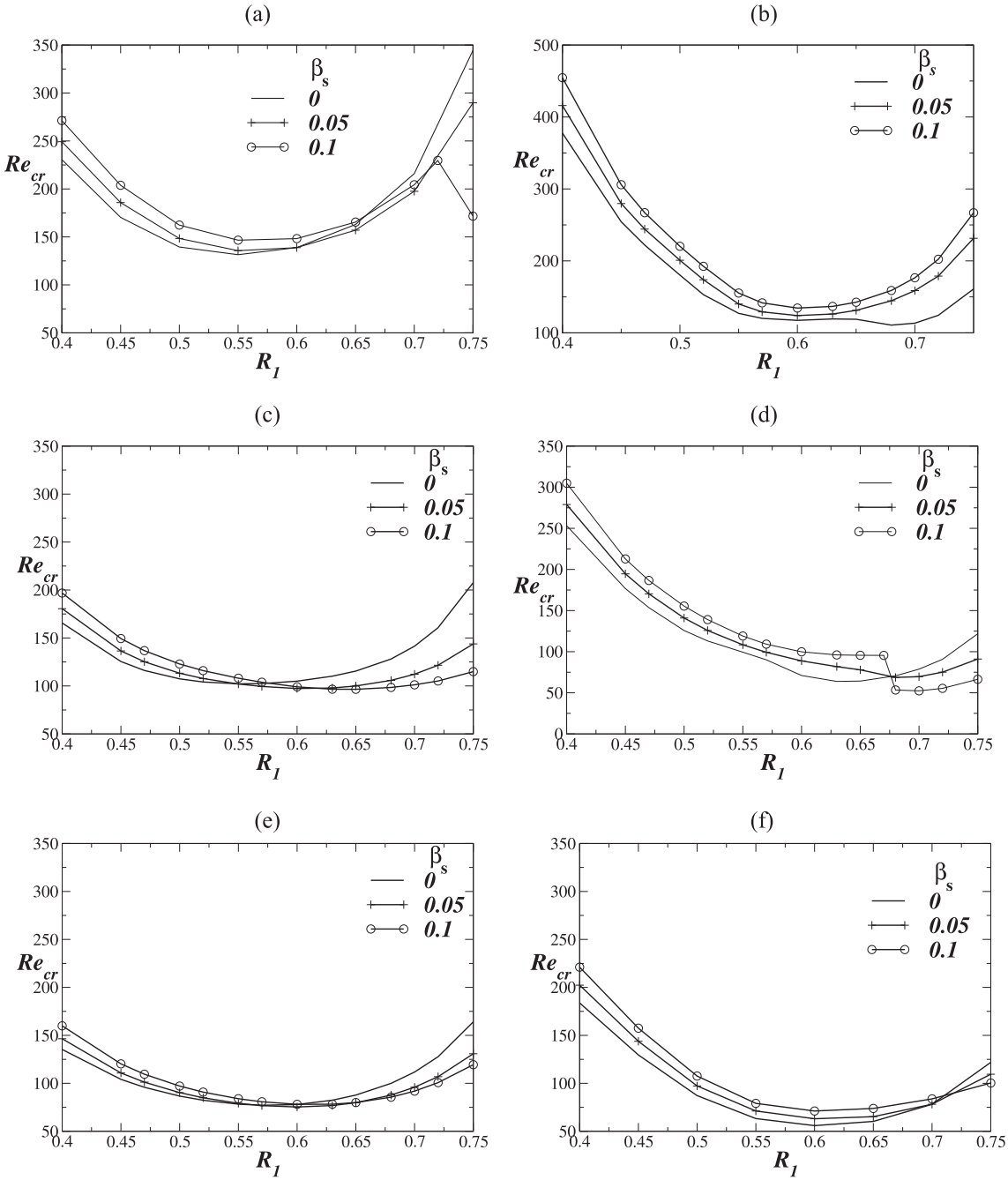

FIG. 7. The critical Reynolds number (Re_{cr}) as a function of the location of the mixed layer (R_1), when the less viscous fluid is nearer to the pipe wall ($R_s = 1$, $R_f = -1.1$). The slip effects are presented (lines with symbols; $\beta_s = 0.05, \beta_s = 0.1$). Solid lines show the results in a rigid pipe ($\beta_s = 0.0$). The other parameters are $Sc = 10$, $q = 0.1$. (a), (c), and (e) show the results for the axisymmetric mode $\beta = 0$, and (b), (d), and (f) show the results for the swirl mode $\beta = 1$.

centerline) which shows the destabilizing effect of the diffusivity ratio δ. But, when the mixed layer is located closer to the pipe wall and with $R_1 > R_{1cr}$, the reverse trend is observed (with an exception for $\delta = 10$ as mentioned earlier). At any δ, slip destabilizes (stabilizes) both the modes when $R_1 > R_{1cr}$ ($R_1 < R_{1cr}$) by decreasing (increasing) the critical Reynolds numbers (with an exception for $\delta = 10$, $\beta = 1$; in this case, slip always stabilizes the swirl mode).

C. Role of mixed layer thickness

One is curious to know if the stability characteristics are affected by the thickness of the mixed layer and some information in this regard is presented in Fig. 8 and Table V. The dispersion relation for the axisymmetric mode [$\beta = 0$; Fig. 8(a)] and the swirl mode [$\beta = 1$; Fig. 8(b)] is presented for non-zero thickness of the interface, when the mixed layer is located nearer the slippery wall ($R_1 = 0.75$). The other parameters are fixed at $Sc = 10$, $\delta = 20$, and $Re = 500$ with $R_f = -1.1$ and $R_s = 1$. The slip effects are incorporated [$\beta_s = 0$, no symbol; and $\beta_s = 0.07$ (△)]. The solid (dashed) lines present the growth rates for $q = 0.1$ ($q = 0.05$). An increase in the mixed layer thickness results in shifting of the maximum growth rate to longwaves, in a rigid as well as in a slippery pipe; the shortwaves are stabilized and the growth rates are decreased. An

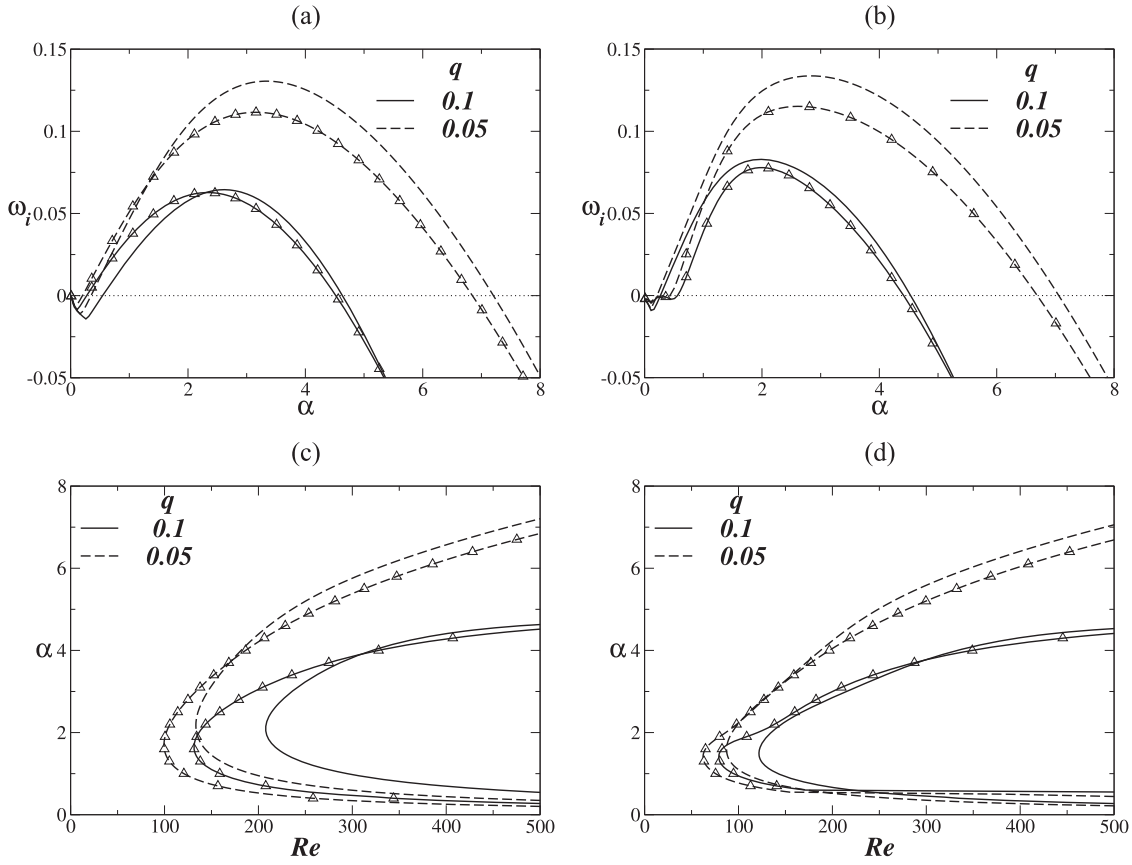

FIG. 8. The destabilizing effect of the thinner mixed layer (q) and the effect of wall slip (β_s) when the less viscous fluid is in the annular region ($R_f = -1.1$, $R_s = 1$), [(a) and (b)] dispersion curves for $Re = 500$, [(c) and (d)] neutral boundaries for the axisymmetric mode ($\beta = 0$) and the swirl mode ($\beta = 1$), respectively, with the rest of the parameters $R_1 = 0.75$, $Sc = 10$, $\delta = 20$. The $\triangle$ represents $\beta_s = 0.07$. The solid and dashed lines without symbols represent the results for $\beta_s = 0$. $\beta_s(=0, 0.07)$ effects alter with the Reynolds number (Re).

increase in slip suppresses the maximum growth rate; the bandwidth of unstable wavenumbers is smaller for a thicker mixed layer. The swirl mode displays slightly higher growth rates [Fig. 8(b)].

The neutral stability curves plotted in the α-Re plane for $\beta = 0$ [Fig. 8(c)] and $\beta = 1$ [Fig. 8(d)] clearly show the destabilizing effect of the thinner mixed layer. The mixed layer is located closer to the slippery wall ($R_1 = 0.75$). Table V presents the critical Reynolds numbers for a thinner ($q = 0.05$) and thicker ($q = 0.1$) mixed layer as the slip varies ($\beta_s = 0$, 0.05, and 0.07). The critical Reynolds number is higher for the axisymmetric mode ($\beta = 0$) then for the swirl mode ($\beta = 1$) for $q = 0.05$ and $q = 0.1$. An increase in slip decreases the critical Reynolds number for the axisymmetric and swirl modes, indicating the destabilizing role of slip for the set of parameters considered.

TABLE V. Effects of the mixed layer thickness (q) on the critical Reynolds number (Re_{cr}) for flow in a rigid/slippery pipe. Values are obtained from Fig. 8.

	$q = 0.1$, $\beta = 0$	$q = 0.05$, $\beta = 1$	$q = 0.1$, $\beta = 0$	$q = 0.05$, $\beta = 1$
$\beta_s = 0$	201.73	121.77	133.38	87.30
$\beta_s = 0.05$	143.86	91.06	105.212	70.02
$\beta_s = 0.07$	131.38	78.94	99.43	62.24

D. Role of Schmidt number on DD instability

We now consider the effects of the Schmidt number (Sc) on the growth rates of the axisymmetric modes ($\beta = 0$) for DD flow in a rigid pipe ($\beta_s = 0$) and in a slippery pipe ($\beta_s = 0.05$). Figure 9 presents the growth rates as a function of α

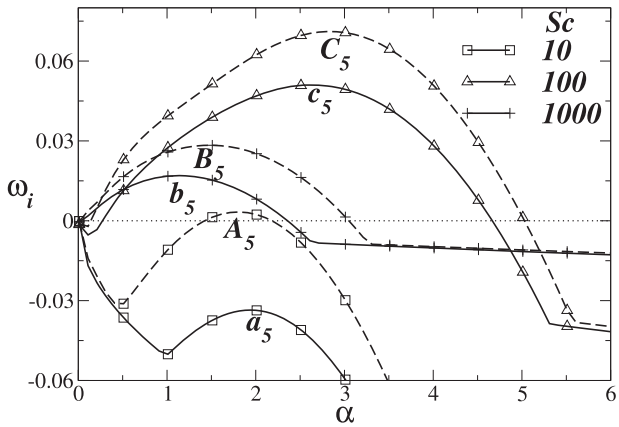

FIG. 9. Effects of the Schmidt number (Sc) on the growth rate of axisymmetric modes ($\beta = 0$) as a function of wavenumber (α) with the other parameters as $Re = 150$, $q = 0.1$, $R_s = 1$, $R_f = -1.1$, $R_1 = 0.75$, $\delta = 20$. Solid and dashed curves represent the case of rigid ($\beta_s = 0$) and slippery ($\beta_s = 0.05$) pipes, respectively. The points a_5, b_5, and c_5 correspond to $\alpha = 1.95$, 2.61, and 1.11, respectively, when $\beta_s = 0$. The points A_5, B_5, and C_5 correspond to $\alpha = 1.8$, 2.81, and 1.51, respectively, when $\beta_s = 0.05$.

TABLE VI. Energy budget for the points a_5, b_5, c_5, A_5, B_5, and C_5 in Fig. 9.

Points	α	ω_i	$\dot{E}$	$\mathcal{P}$	$-\mathcal{D}$	$\mathcal{A}$	$\mathcal{B}_r$	$\mathcal{B}_z$	$\mathcal{C}$
a_5	1.95	−0.033 51	−0.0040	−0.0017	−0.1596	0.0003	0.1671	−0.0058	−0.0043
c_5	2.61	0.050 98	0.0043	0.0094	−0.2830	0.0003	0.2860	−0.0062	−0.0023
b_5	1.11	0.016 94	−0.0013	0.0029	−0.5162	0.0000	0.5149	−0.0008	−0.0021
A_5	1.80	0.003 33	0.0100	−0.0025	−0.1415	0.0003	0.1617	−0.0051	−0.0028
C_5	2.81	0.071 06	0.0116	0.0129	−0.2865	0.0004	0.2943	−0.0080	−0.0015
B_5	1.51	0.028 36	0.0026	0.0045	−0.5446	0.0001	0.5461	−0.0017	−0.0018

for different values of Sc; the other parameters are same as in Fig. 3(a). It is observed that the Schmidt number has a non-monotonic effect for a DD flow in rigid as well as in slippery pipes.

At higher Sc(=1000), the long-waves are destabilized for DD flow in a pipe (rigid and slippery). At any Sc, the growth rate is higher and the bandwidth of unstable wavenumbers is larger for flow in a slippery pipe. This non-monotonic behavior with respect to Sc can be clearly understood through the energy budget analysis, and this is presented in Table VI for $Re = 150$, $q = 0.1$, $R_s = 1$, $R_f = -1.1$, $R_1 = 0.75$, $\delta = 20$, $\beta_s = 0$, and $\beta_s = 0.05$. At this Re, the contributions from $\mathcal{B}_r$ and $\mathcal{D}$ almost cancel out; $\mathcal{A}$, $\mathcal{B}_z$, and $\mathcal{C}$ are negligible. The contribution from $\mathcal{P}$ is seen to be responsible for the non-monotonic behavior of Sc which is exhibited in Fig. 9. This is displayed by DD flow in a rigid as well as in a slippery pipe.

At a fixed Reynolds number, as Sc increases, diffusion slows down. There are some intermediate Schmidt numbers beyond which when Sc increases, the growth rate of the dominant mode of instability is suppressed. This can be attributed to the non-monotonic behavior displayed by the Reynolds stress term, $\mathcal{P}$ (see Table VI). It can be seen that with the increase in Sc, $\mathcal{P}$ increases initially but beyond some Sc, it begins to decrease due to the insufficient rate of energy transferred from base flow to the perturbations. As a result, growth rate exhibits non-monotonic behavior as Sc is increased. This may be attributed to the contribution from the shear stress that arises due to slip.

Note from Table VI that for a fixed Re and Sc, the rate of energy transfer from the base flow to the perturbations is enhanced with slip which results in a higher growth rate in a slippery duct. Further, as Sc increases, the contribution from $\mathcal{P}$ is higher in a slippery pipe than that in a rigid pipe.

Figures 10 and 11 also confirm the above conclusions. The contribution from all the terms to the energy budget are presented as a function of Re, when $Sc = 10$ and $\beta_s = 0.05$ in a slippery pipe and all the other parameters are as in Table VI. The above results for $Sc = 100$ and $Sc = 1000$ are also obtained but are not shown here as the trend is observed to be similar to that for $Sc = 10$. From Fig. 10, it is observed that, at any Re, the positive and negative contributions from $\mathcal{B}_r$ and $\mathcal{D}$ almost cancel out each other and $\mathcal{P}$ is the dominant contributing term. Figure 11 presents the effects of the Schmidt number on the contribution to energy budget from the Reynolds stress term that determines the rate of transfer of energy to the perturbation from the basic flow ($\mathcal{P}$). Note that the contribution to the Reynolds stress production is from the derivative of base flow velocity. It is clear that there is a window of Reynolds numbers where $\mathcal{P}$ is non-monotonic with respect to Sc ($150 < Re < 700$ for flow in a rigid pipe and $150 < Re < 900$ for flow in a slippery pipe), and beyond this

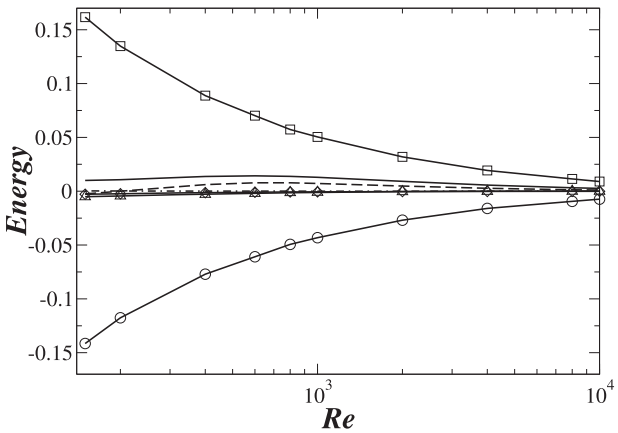

FIG. 10. The terms of the energy equation for flow in a slippery pipe ($\beta_s = 0.05$) as a function of Reynolds number (Re) with $Sc = 10$, $q = 0.1$, $R_s = 1$, $R_f = -1.1$, $\delta = 20$, $\beta = 0$, and $R_1 = 0.75$. The dominant contributing term is the Reynolds stress term ($\mathcal{P}$); the terms $\mathcal{B}_r$ and $\mathcal{D}$ almost cancel each other. Solid line represents $\dot{E}$, dashed line represents $\mathcal{P}$, dashed-dotted line represents $\mathcal{A}$, ◇ represents $\mathcal{C}$, △ represents $\mathcal{B}_z$, □ represents $\mathcal{B}_r$, o represent $-\mathcal{D}$.

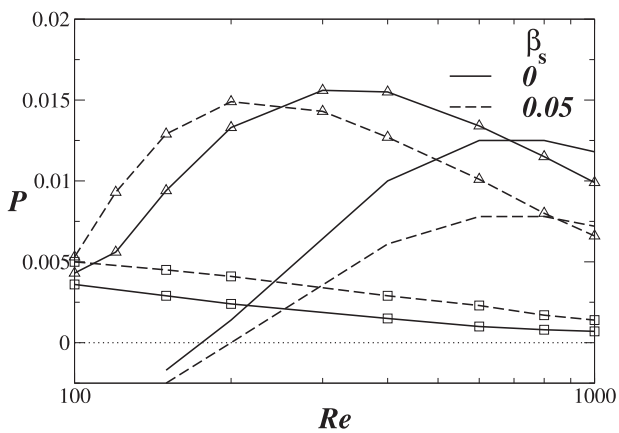

FIG. 11. The Reynolds stress term $\mathcal{P}$ as a function of the Reynolds number (Re) for different values of Sc with other parameters same as in Fig. 10. $\mathcal{P}$ is non-monotonic with respect to Sc in the window $150 < Re < 700$ for DD flow in a rigid pipe (solid lines; $\beta_s = 0$) and in the window $150 < Re < 900$ for DD flow in a slippery pipe (dashed lines; $\beta_s = 0.05$). The solid or dashed lines without symbols correspond to $Sc = 10$ and with triangles (△) and squares (□) correspond to $Sc = 100$ and $Sc = 1000$, respectively.

$Re \simeq 700$ ($Re \simeq 900$), $\mathcal{P}$ is monotonically decreasing for the rigid (slippery) case.

In this manuscript, the effects of slip on core annular pipe flows are considered. The slip boundary condition comes into action not only in micro- or nanofluidics but also in large scale systems involving hydrophobic walls. The experiment carried out by Watanabe *et al.*[41] reports that a drag reduction phenomenon takes place for water flowing in a pipe with water-repellent walls of a fixed diameter. They showed that the shear stress is directly proportional to the wall slip. The maximum reduction occurs at Reynolds number 2×10^5 approximately. The velocity profiles in highly water-repellent wall pipe ware presented for the Reynolds number of the order of 1000 (in their Fig. 9). Their calculated and experimental values of the friction factor over the laminar flow range showed an excellent agreement. The shift in the velocity profile observed in this study was also observed by Tretheway and Meinhart.[42] for hydrophobic microchannels. This suggests that in the case of a significantly larger hydrophobic duct, the Reynolds number may rise up to O(1000) or even O(10 000).

VI. CONCLUSIONS

The present investigation addresses the temporal instability of viscosity stratified miscible core-annular flows (DD systems) in a slippery pipe. The results demonstrate that miscible core-annular flows in a slippery pipe are linearly unstable towards longwave and intermediate wave disturbances, for a wide range of governing parameters. When the less viscous fluid is in the annular region and the mixed layer is closer to the slippery wall, then, while the DD flow is unstable, the equivalent SC flow is stable, showing that the stability characteristics are analogous to that in a rigid pipe (Fig. 3). Further, an increase in the relative diffusion rate (δ) enhances the instability of an axisymmetric mode in a DD system with more destabilization due to slip effects. At moderate to high diffusivity ratios, the swirl mode displays the same scenario, but at small diffusion ratios, slip has a stabilizing effect on the swirl mode (Fig. 7). Diffusion effects are observed to be non-monotonic (as in the rigid wall case) for the DD system (Fig. 9), whereas in a SC system, its effects are monotonic (not shown). The energy transfer from base flow to the perturbation, namely, the Reynolds stress is responsible for this non-monotonic effect of Sc. The source of instability in this configuration is due to an increase in the slope of base flow velocity. The location of the mixed layer also has a non-monotonic effect on the stability characteristics; slip has a dual role of stabilizing or destabilizing depending on whether the mixed layer is nearer the centerline or closer to the pipe wall (Figs. 3 and 7). The DD flow in a plane slippery channel is more stable than that in core-annular flow in a slippery pipe [Fig. 9 in the work of Ghosh *et al.*;[13] Fig. 6(a) in the present study]. The energy budget analysis reveals clearly that the mechanism of energy transfer from the base flow to the disturbance depends on the Schmid number (Sc) and slip (β_s). The transfer of energy may be through the Reynolds stress term (Figs. 9–11) or through stresses due to gradient of viscosity perturbation in the radial direction (Fig. 3). Note that the preliminary DNS computations, (Fig. 1), not only confirm the linear stability results but provide information in the nonlinear regime. The results show that the slip delays the occurrence of instability in a DD core-annular flow for some range of parameter values while it does the reverse for other range of parameters of interest in the present study. Slip plays a dual role of stabilizing or destabilizing the miscible core annular DD flow in a pipe. For the flow configuration with a mixed layer closer to the wall when the faster diffusing scalar is stabilizing and the slower diffusing scalar is destabilizing, we observe that an increase in the slip length (which arises due to slip at the wall) decreases the critical Reynolds number. It is possible to further destabilize the flow configuration by decreasing the mixed layer thickness (Table V). This clearly shows that both the slip length and the mixed layer thickness play a crucial role on the stability characteristics of the DD miscible core annular flow in a pipe.

The present study has relevance in micro-electro mechanical systems, in which the velocity slip boundary condition is more appropriate than the no-slip condition, to describe the flow dynamics. For example, rarefied gas flows can be observed in MEMS where the characteristic size of the system is around or less than a few micrometers. The characteristic length in such systems is very small resulting in the range of Knudsen numbers, characterizing velocity slip to be small ($10^{-3} < K_n < 0.1$), in spite of the gas being dense and the mean free path of the gas molecules being very small. Slip flows are governed by Navier-Stokes equations with a slip velocity between the gas and the solid boundary[43] in these systems. Pan *et al.*[43] have carried out a qualitative analysis for the above system and have calculated the slip coefficient which is very useful for slip flow analyses in MEMS, using Navier-Stokes equations.

The study also gains its significance due to the dual role played by slip at the wall, as it suggests an effective way of controlling miscible core-annular flow in a rigid pipe. The study can be extended to consider the non-modal stability analysis for core-annular flows so that there is a possibility for quantifying the wall slip effects of the present study on the non-modal stability analysis.

ACKNOWLEDGMENTS

We take this opportunity to thank the reviewers for their useful suggestions and comments. The authors also thank the editor for his suggestions and encouraging remarks.

APPENDIX A: BASE STATE

The base state (U_z, μ_0) corresponds to a steady locally parallel, fully developed flow [$U_r = 0, U_\theta = 0, U_z = U_z(r)$ and P is linear in z] satisfying

$$\frac{1}{r}\frac{\partial}{\partial r}\left[r\mu_0\frac{\partial U_z}{\partial r}\right] = Re\frac{dP}{dz} \tag{A1}$$

and the boundary conditions

$$U_z = -\beta_s\frac{\partial U_z}{\partial r} \quad \text{on} \quad r = 1, \tag{A2}$$

$$\frac{\partial U_z}{\partial r} = 0 \quad \text{on} \quad r = 0. \tag{A3}$$

The condition $\int_0^1 U_z r dr = 1$ is used to fix the pressure gradient dP/dz. Here $\mu_0 = \exp(R_s s_0 + R_f f_0)$, where the scalars s_0 and f_0 are chosen to be of fifth degree polynomials[10,11] and this assumes the continuity up to the second derivative for the concentration of the scalars at $r = R_1$ and $r = R_1 + q$,

$$\begin{aligned} s_0 = f_0 &= 0, \qquad 0 \le r \le R_1, \\ s_0 = f_0 &= \sum_{i=1}^{6} a_i r^{i-1}, \quad R_1 \le r \le R_1 + q, \\ s_0 = f_0 &= 1, \qquad R_1 + q \le r \le 1, \end{aligned} \tag{A4}$$

where $a_i (i = 1–6)$ are given by

$$\begin{aligned} a_1 &= -\frac{{R_1}^3}{q^5}\left(6R_1^2 + 15R_1 q + 10q^2\right), \quad a_2 = \frac{30{R_1}^2}{q^5}(R_1+q)^2, \\ a_3 &= -\frac{30R_1}{q^5}(R_1+q)(2R_1+q), \quad a_4 = \frac{10}{q^5}\left(6R_1^2 + 6R_1 q + q^2\right), \\ a_5 &= -\frac{15}{q^5}(2R_1+q), \quad \text{and} \quad a_6 = \frac{6}{q^5}. \end{aligned} \tag{A5}$$

Sahu[11] has remarked that the base state profiles generated by using sufficiently smooth concentration profiles with $s_0 = f_0 = 0.5 + 0.5\,\mathrm{erf}\left(\frac{r-R_1-0.5q}{0.25q}\right)$ considered by Selvam *et al.*[8] are similar to those obtained using (A4) and (A5). The validity of the choice of Eqs. (A4) and (A5) is presented in Appendix C in the work of Sahu.[11]

The base velocity profiles are plotted in Fig. 12 for DD flow configurations with $R_s = 1$, when the mixed layer of thickness $q = 0.1$ is located near the pipe wall ($R_1 = 0.7$). The presence of slip provokes larger velocities near the pipe wall. The axial velocity in the mixed layer ($0.7 < r < 0.8$) is more for the DD flow system with less viscous fluid ($R_f = -1.1$, $R_s = 1$; dashed line) as compared to that with more viscous fluid ($R_f = -0.9$, $R_s = 1$; solid line) in the annular region. This is observed for flow in a rigid ($\beta_s = 0$) as well as in a slippery ($\beta_s \neq 0$) pipe. Slip at the wall enhances this axial velocity in the mixed layer. The results for a rigid pipe ($\beta_s = 0$) agree with those in Fig. 2 in the work of Sahu.[11] The centerline velocity for the DD flow system in a rigid pipe exceeds that in a slippery pipe; it is more when the high viscous fluid is in the annular region than when the less viscous fluid is in the annular region. The wall shear is more in a rigid pipe than in a slippery pipe. Further, the wall shear in a slippery pipe ($\beta_s = 0.05$, $\beta_s = 0.1$) is less for a configuration with the less viscous fluid occupying the annular region than the one with more viscous fluid in the annular region.

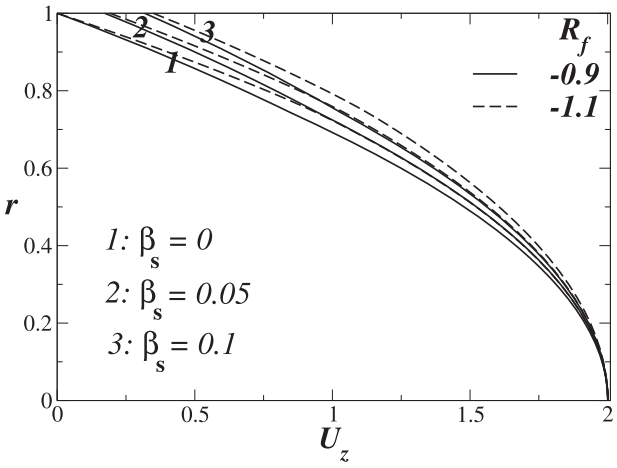

FIG. 12. Basic velocity profiles in a DD flow configuration when $R_1 = 0.7$ and $q = 0.1$ with less viscous fluid ($R_f = -1.1$, $R_s = 1$; dashed line) and more viscous fluid ($R_f = -0.9$, $R_s = 1$; solid line) in the annular region.

APPENDIX B: ENTRIES IN MATRIX A AND B

$$\mathcal{A}_{11} = \alpha U_z + \frac{i\mu_0}{Re}\left\{\mathcal{D}^2 + \frac{\mathcal{D}}{r} - \left(\frac{\beta^2+1}{r^2} + \alpha^2\right)\right\} + \frac{2i\mu_0'}{Re}\mathcal{D},$$

$$\mathcal{A}_{12} = -\frac{2i\beta\mu_0}{r^2 Re}, \quad \mathcal{A}_{14} = -\mathcal{D},$$

$$\mathcal{A}_{15} = \frac{iU_z'\alpha}{R}\mu_0 R_s, \mathcal{A}_{16} = \frac{iU_z'\alpha}{R}\mu_0 R_f,$$

$$\mathcal{A}_{21} = -\frac{2i\beta\mu_0}{r^2 Re} - \frac{i\beta\mu_0'}{rRe},$$

$$\mathcal{A}_{22} = \alpha U_z + \frac{i\mu_0}{Re}\left\{\mathcal{D}^2 + \frac{\mathcal{D}}{r} - \left(\frac{\beta^2+1}{r^2} + \alpha^2\right)\right\} + \frac{i\mu_0'}{Re}\left(\mathcal{D} - \frac{1}{r}\right), \mathcal{A}_{24} = \frac{\beta}{r},$$

$$\mathcal{A}_{31} = U_z' - \frac{i\mu_0'\alpha}{Re}, \mathcal{A}_{33} = \alpha U_z + \frac{i\mu_0}{Re}\left\{\mathcal{D}^2 + \frac{\mathcal{D}}{r} - \left(\frac{\beta^2}{r^2} + \alpha^2\right)\right\} + \frac{i\mu_0'}{Re}\mathcal{D}, \mathcal{A}_{34} = \alpha,$$

$$\mathcal{A}_{35} = \frac{iU_z'}{Re}\left(R_s\mu_0 + R_s\mu_0'\right) + \frac{iR_s\mu_0}{Re}\left(U_z'' + \frac{U_z'}{r}\right),$$

$$\mathcal{A}_{36} = \frac{iU_z'}{Re}\left(R_f\mu_0 + R_f\mu_0'\right) + \frac{iR_f\mu_0}{Re}\left(U_z'' + \frac{U_z'}{r}\right),$$

$$\mathcal{A}_{41} = r\mathcal{D} + 1, \mathcal{A}_{42} = \beta, \mathcal{A}_{43} = r\alpha,$$

$$\mathcal{A}_{51} = s_0', \mathcal{A}_{55} = \alpha U_z + \frac{i}{ReSc}\left\{\mathcal{D}^2 + \frac{\mathcal{D}}{r} - \left(\frac{\beta^2}{r^2} + \alpha^2\right)\right\},$$

$$\mathcal{A}_{61} = f_0', \mathcal{A}_{66} = \alpha U_z + \frac{i\delta}{ReSc}\left\{\mathcal{D}^2 + \frac{\mathcal{D}}{r} - \left(\frac{\beta^2}{r^2} + \alpha^2\right)\right\},$$

$$\mathcal{B}_{11} = \mathcal{B}_{22} = \mathcal{B}_{23} = \mathcal{B}_{55} = \mathcal{B}_{66} = 1.$$

Here $\mathcal{D} = d/dr$.

[1] R. Govindarajan and K. C. Sahu, "Instabilities in viscosity-stratified flow," Annu. Rev. Fluid Mech. **46**, 331–353 (2014).
[2] D. Joseph and Y. Renardy, "Fundamentals of Two-Fluid Dynamics: Part II: Lubricated Transport," *Drops Miscible Fluids* (Springer Science & Business Media, 1993).
[3] D. D. Joseph, R. Bai, K. Chen, and Y. Y. Renardy, "Core-annular flows," Annu. Rev. Fluid Mech. **29**, 65–90 (1997).
[4] B. T. Ranganathan and R. Govindarajan, "Stabilization and destabilization of channel flow by location of viscosity-stratified fluid layer," Phys. Fluids **13**, 1–3 (2001).
[5] R. Govindarajan, "Effect of miscibility on the linear instability of two-fluid channel flow," Int. J. Multiphase Flow **30**, 1177–1192 (2004).
[6] P. Ern, F. Charru, and P. Luchini, "Stability analysis of a shear flow with strongly stratified viscosity," J. Fluid Mech. **496**, 295–312 (2003).
[7] S. V. Malik and A. P. Hooper, "Linear stability and energy growth of viscosity stratified flows," Phys. Fluids **17**, 024101 (2005).

[8]B. Selvam, S. Merk, R. Govindarajan, and E. Meiburg, "Stability of miscible core–annular flows with viscosity stratification," J. Fluid Mech. **592**, 23–49 (2007).
[9]K. C. Sahu, H. Ding, P. Valluri, and O. Matar, "Linear stability analysis and numerical simulation of miscible two-layer channel flow," Phys. Fluids **21**, 042104 (2009).
[10]K. C. Sahu and R. Govindarajan, "Linear stability of double-diffusive two-fluid channel flow," J. Fluid Mech. **687**, 529–539 (2011).
[11]K. C. Sahu, "Double-diffusive instability in core–annular pipe flow," J. Fluid Mech. **789**, 830–855 (2016).
[12]S. Ghosh, R. Usha, and K. C. Sahu, "Linear stability analysis of miscible two-fluid flow in a channel with velocity slip at the walls," Phys. Fluids **26**, 014107 (2014).
[13]S. Ghosh, R. Usha, and K. C. Sahu, "Double-diffusive two-fluid flow in a slippery channel: A linear stability analysis," Phys. Fluids **26**, 127101 (2014).
[14]O. I. Vinogradova, K. Koynov, A. Best, and F. Feuillebois, "Direct measurements of hydrophobic slippage using double-focus fluorescence cross-correlation," Phys. Rev. Lett. **102**, 118302 (2009).
[15]C. Lee, C.-H. Choi *et al.*, "Structured surfaces for a giant liquid slip," Phys. Rev. Lett. **101**, 064501 (2008).
[16]J. Ou, B. Perot, and J. P. Rothstein, "Laminar drag reduction in microchannels using ultrahydrophobic surfaces," Phys. Fluids **16**, 4635–4643 (2004).
[17]J. M. Gersting, Jr., "Hydrodynamic stability of plane porous slip flow," Phys. Fluids **17**, 2126–2127 (1974).
[18]A. Spille, A. Rauh, and H. Bühring, "Critical curves of plane Poiseuille flow with slip boundary conditions," Nonlin. Phenom. Complex Syst. **3**(2), 171–173 (2000).
[19]C.-J. Gan and Z.-N. Wu, "Short-wave instability due to wall slip and numerical observation of wall-slip instability for microchannel flows," J. Fluid Mech. **550**, 289–306 (2006).
[20]E. Lauga and C. Cossu, "A note on the stability of slip channel flows," Phys. Fluids **17**, 088106 (2005).
[21]R. Ling, C. Jian-Guo, and Z. Ke-Qin, "Dual role of wall slip on linear stability of plane Poiseuille flow," Chin. Phys. Lett. **25**, 601 (2008).
[22]K. C. Sahu, A. Sameen, and R. Govindarajan, "The relative roles of divergence and velocity slip in the stability of plane channel flow," Eur. Phys. J. Appl. Phys. **44**, 101–107 (2008).
[23]J. C. Maxwell, "On stresses in rarified gases arising from inequalities of temperature," Philos. Trans. R. Soc. London **170**, 231–256 (1879).
[24]G. Karniadakis, A. Beskok, and M. Gad-el Hak, "Micro flows: Fundamentals and simulation," Appl. Mech. Rev. **55**, B76 (2002).
[25]X.-Y. You and J.-R. Zheng, "Stability of liquid-liquid stratified microchannel flow under the effects of boundary slip," Int. J. Chem. React. Eng. **7**, 1–12 (2009).
[26]C. Neto, D. R. Evans, E. Bonaccurso, H.-J. Butt, and V. S. Craig, "Boundary slip in Newtonian liquids: A review of experimental studies," Rep. Prog. Phys. **68**, 2859 (2005).
[27]E. Lauga, M. Brenner, and H. Stone, "Microfluidics: The no-slip boundary condition," *in Springer Handbook of Experimental Fluid Mechanics* (Springer, 2007), pp. 1219–1240.
[28]X. Zhang, F. Shi, J. Niu, Y. Jiang, and Z. Wang, "Superhydrophobic surfaces: From structural control to functional application," J. Mater. Chem. **18**, 621–633 (2008).
[29]J. P. Rothstein, "Slip on superhydrophobic surfaces," Annu. Rev. Fluid Mech. **42**, 89–109 (2010).
[30]A. Kumar, S. Datta, and D. Kalyanasundaram, "Permeability and effective slip in confined flows transverse to wall slippage patterns," Phys. Fluids **28**, 082002 (2016).
[31]C.-O. Ng, H. C. Chu, and C. Wang, "On the effects of liquid-gas interfacial shear on slip flow through a parallel-plate channel with superhydrophobic grooved walls," Phys. Fluids **22**, 102002 (2010).
[32]C.-H. Choi, U. Ulmanella, J. Kim, C.-M. Ho, and C.-J. Kim, "Effective slip and friction reduction in nanograted superhydrophobic microchannels," Phys. Fluids **18**, 087105 (2006).
[33]V. Pruša, "On the influence of boundary condition on stability of Hagen–Poiseuille flow," Comput. Math. Appl. **57**, 763–771 (2009).
[34]Z. Ding, T. N. Wong, R. Liu, and Q. Liu, "Viscous liquid films on a porous vertical cylinder: Dynamics and stability," Phys. Fluids **25**, 064101 (2013).
[35]T. Min and J. Kim, "Effects of hydrophobic surface on stability and transition," Phys. Fluids **17**, 108106 (2005).
[36]R. S. Voronov, D. V. Papavassiliou, and L. L. Lee, "Review of fluid slip over superhydrophobic surfaces and its dependence on the contact angle," Ind. Eng. Chem. Res. **47**, 2455–2477 (2008).
[37]T. D. Blake, "Slip between a liquid and a solid: D.M. Tolstoi's (1952) theory reconsidered," Colloids Surf. **47**, 135–145 (1990).
[38]O. I. Vinogradova, "Drainage of a thin liquid film confined between hydrophobic surfaces," Langmuir **11**, 2213–2220 (1995).
[39]P. J. Schmid and D. S. Henningson, *Stability and Transition in Shear Flows* (Springer Science & Business Media, 2012), Vol. 142.
[40]C. Canuto, M. Y. Hussaini, A. M. Quarteroni, A. Thomas, Jr. *et al.*, *Spectral Methods in Fluid Dynamics* (Springer Science & Business Media, 2012).
[41]K. Watanabe, Y. Udagawa, and H. Udagawa, "Drag reduction of Newtonian fluid in a circular pipe with a highly water-repellent wall," J. Fluid Mech. **381**, 225–238 (1999).
[42]D. C. Tretheway and C. D. Meinhart, "Apparent fluid slip at hydrophobic microchannel walls," Phys. Fluids **14**, L9–L12 (2002).
[43]L. Pan, G. Liu, and K. Lam, "Determination of slip coefficient for rarefied gas flows using direct simulation Monte Carlo," J. Micromech. Microeng. **9**, 89 (1999).